Electronic Supplementary Material (ESI) for Physical Chemistry Chemical Physics.
This journal is © the Owner Societies 2022

Supporting Information

Structure Property Investigations in Urea Tethered Iodinated Triphenylamines

Muhammad Saddam Hossain,[a] Fiaz Ahmed,[a] Stavros G. Karakalos,[b] Mark D. Smith,[a] Namrata Pant, [c] Sophya Garashchuk,[a] Andrew B. Greytak,[a] Pablo Docampo,[c] and Linda S. Shimizu[a]*

[a]Department of Chemistry and Biochemistry, University of South Carolina, Columbia, South Carolina 29208, United States.

[b]College of Engineering and Computing, University of South Carolina, Columbia South Carolina 29208, USA.

[c]School of Chemistry, University of Glasgow, Glasgow, G12 8QQ.

Fax: 803-777-9521; Tel: 803-777-2066

Email: SHIMIZLS@mailbox.sc.edu

Contents

List of Figures

List of Tables

GENERAL METHODS: Both commercially available reagents and solvents were purchased from VWR, Sigma-Aldrich, TCI America and, Alfa Aesar and used in synthesis without any further purification. Reagents that are air-sensitive stored under the protection of nitrogen. The round bottom flask was oven-dried for reactions. ^{1}H NMR, ^{13}C NMR spectra were recorded in Bruker Avance 300 or 400 MHz spectrometers. To report the chemical shift in ppm, solvent peaks were used as a reference. High-resolution mass spectra were recorded in a direct exposure probe (DEP) in electron ionization (EI) mode on a waters QTOF-I quadrupole time-of-flight mass spectrometer.

Experimental Procedures

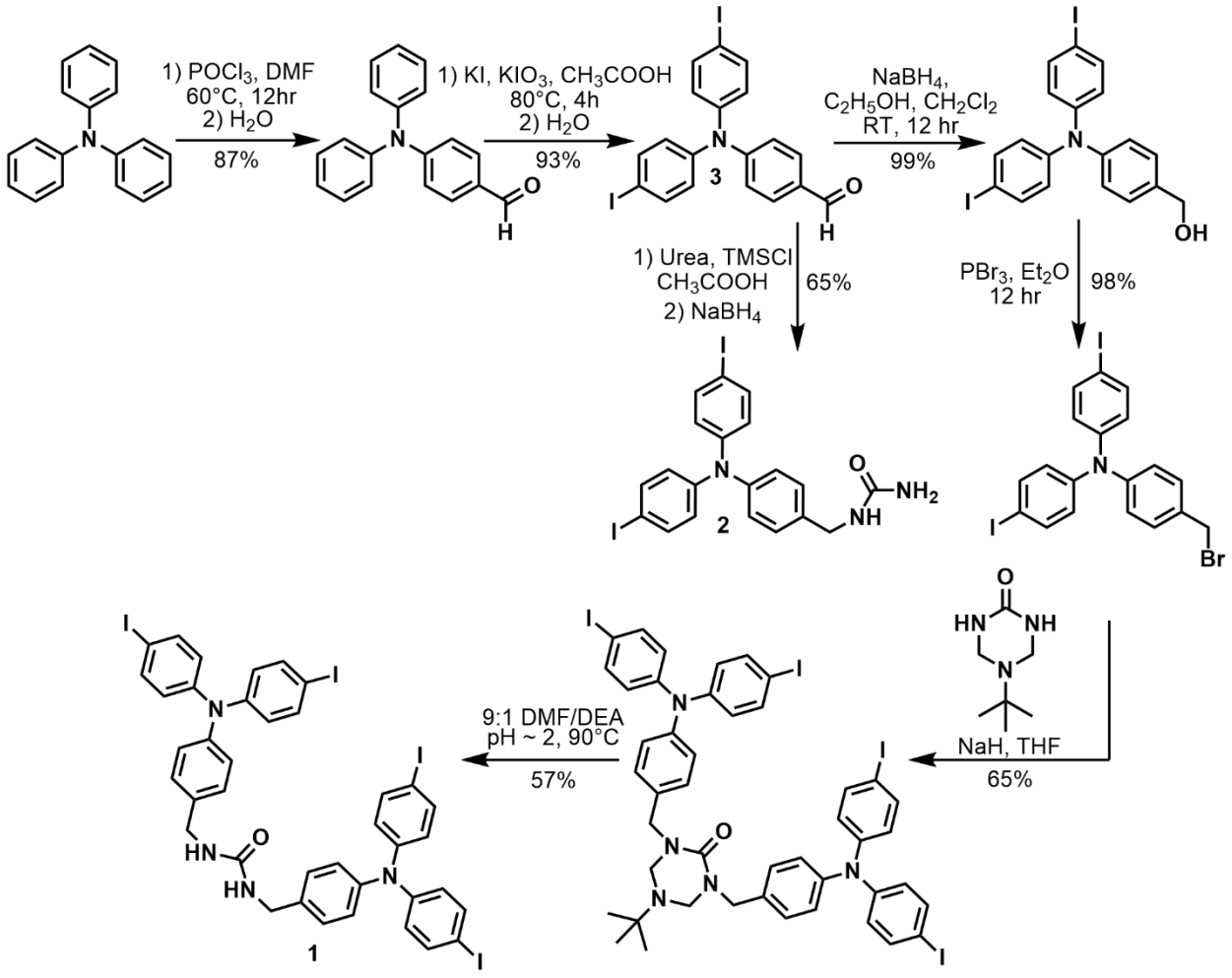

Scheme S1: Synthesis of **1** and urea tethered iodinated **2**, and **3**.

Synthesis of 4-(diphenylamino)benzaldehyde

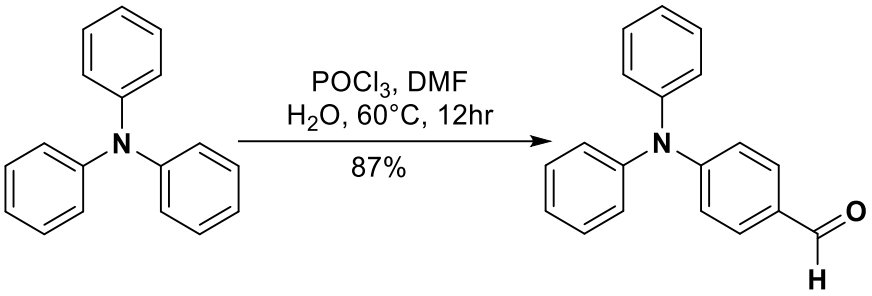

The compound was synthesized according to the previous literature procedures.[1] In an oven-dry round bottom flask, phosphoryl chloride (1.055 mL, 11.34 mmol, 1 equiv.) was added dropwise to N, N-dimethylformamide (0.875 mL, 11.34 mmol, 1 equiv.) at 0°C and let the mixture stirred for 20 minutes at room temperature. For proper safety, an elevated flow rate in the hood and acid glove was used. Next, commercially available triphenylamine (1 g, 4.10 mmol, 0.36 mmol) was dissolved in 10 mL of N, N-dimethylformamide and added to the reaction mixture dropwise and the reaction mixture heated at 40°C for 12 hours. After completion, the reaction mixture cooled to room temperature, 30 mL ice-cold H_2O was added and left in the refrigerator for 2 hours. The resulting precipitant was collected by suction filtration and recrystallized from a minimum amount of ethanol. The final product was obtained as a yellow solid (yield 0.9617 g, 87%). The obtained spectra matched with previous reports.[1] ^{1}H NMR (400 MHz, $CDCl_3$): δ (ppm) d 9.81(s, 1H), 7.68 (d, J = 8.4 Hz, 2H), 7.34 (t, 4H), 7.17-7.19 (m, 6H), 7.02 (d, J = 8.5 Hz, 2H). HRMS (EI): [M+] calculated 273.1154, found, 273.1155.

Synthesis of 4-(bis(4-iodophenyl)amino)benzaldehyde

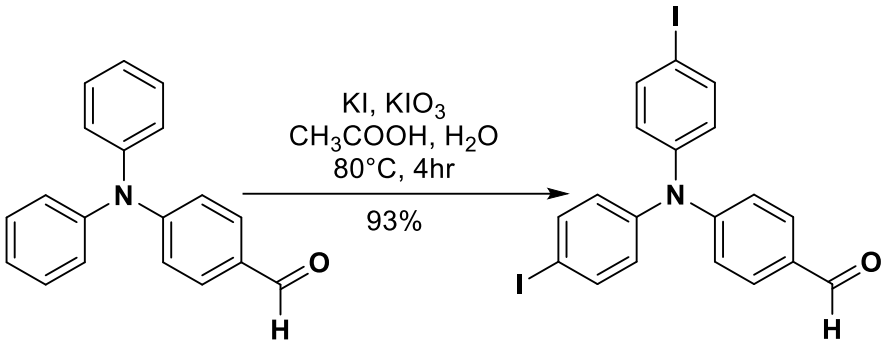

The compound was synthesized according to the previous literature procedure. In a 100 mL round bottom flask, 4-(diphenylamino)benzaldehyde (0.7213 g, 2.638 mmol, 1 equiv.) and potassium iodide (0.591 g, 3.562 mmol, 1.35 equiv.) was added in 10 mL of 9:1 mixture of acetic acid and H_2O. The mixture heated until it reached 80°C. Then potassium iodate (0.565 g, 2.64 mmol, 1 equiv.) was added and the mixture heated at 80°C for 4 hours. After completion, the solution was cooled to room temperature and neutralized with $NaHCO_3$. Then the resulting solution was washed with (3 X 30 mL) methylene chloride, (1 X 30 mL) $Na_2S_2O_3$, and dried over anhydrous MgSO4. The solvent was removed in rotary evaporation and the crude material was purified by column chromatography using 3:1 = Hexane: Ethyl Acetate as eluent. The final product was obtained as a yellow solid (1.29 g, 93%). The obtained spectra matched previous reports.[1] ^{1}H NMR (600 MHz, CDCl3): δ (ppm) 9.84 (s, 1H), 7.71 (d, J = 8.3 Hz, 2H), 7.63 (d, J = 8.5 Hz, 4H), 7.05 (d, J = 8.3 Hz, 2H), 6.89 (d, J = 8.4 Hz, 4H). 13C NMR (150 MHz, CDCl3): δ (ppm)190.35, 152.17, 145.69, 138.85, 131.34, 130.31, 127.60, 120.75, 88.75. MS (FAB): m/z = 524.91 [M+H]+.

Synthesis of 1-(4-(bis(4-iodophenyl)amino)benzyl)urea

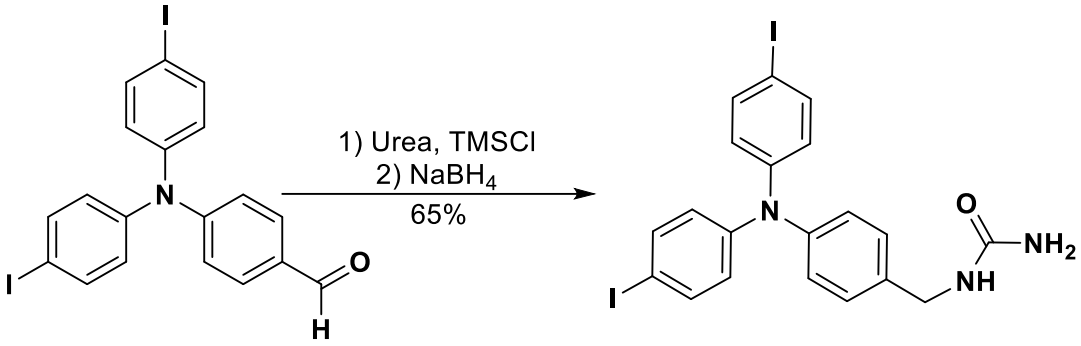

Compound was synthesized according to the previous literature procedure.[2] The previous aldehyde (1.619 g, 3.083 mmol), urea (1.86 g, 30.83 mmol) were dissolved in 50 mL acetic acid and trimethylsilyl chloride (0.58 mL, 4.624 mmol) added. The resulting mixture stirred at room temperature for 12 hours. Then sodium borohydride (0.174 g, 4.624 mmol) were added and continue the stirring for 2 hours. After completion 500 mL of water were added and resulting precipitate collected by filtration. The final product was obtained as beige solid by column chromatography using 1:1 = CH_2Cl_2 : ethyl acetate as eluent (1.138 g, 65%). ^{1}H NMR (300 MHz, (CD_2Cl_2): δ (ppm) 7.52 (d, *J* = 8.8 Hz, 4H), 7.21 (d, *J* = 8.3 Hz, 2H), 7.02 (d, *J* = 8.5 Hz, 2H), 6.80 (d, *J* = 8.8 Hz, 4H), 4.86 (s, *J* = 5.8 Hz, 1H), 4.35 (s, *J* = 5.9 Hz, 2H), 4.29 (d, *J* = 5.9 Hz, 2H). ^{13}C NMR (75 MHz, $(CD_3)_2SO$-*d*$_6$) δ (ppm) 158.62, 146.70, 144.62, 138.08, 137.13, 128.60, 125.20, 125.08, 86.08, 42.32. HRMS (ES): [M+] calculated 568.9461; found: 568.9475

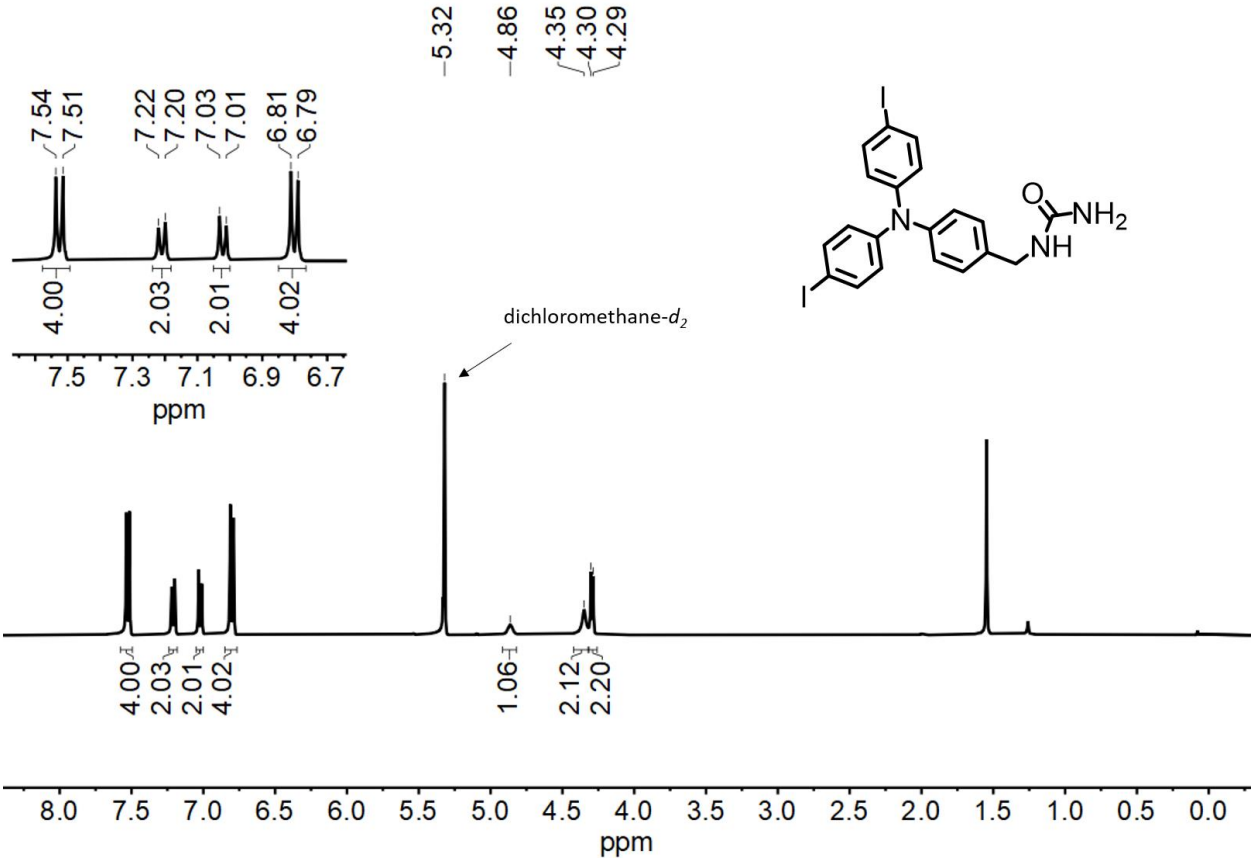

Figure S1. ^{1}H NMR (CD_2Cl_2, 300 MHz)

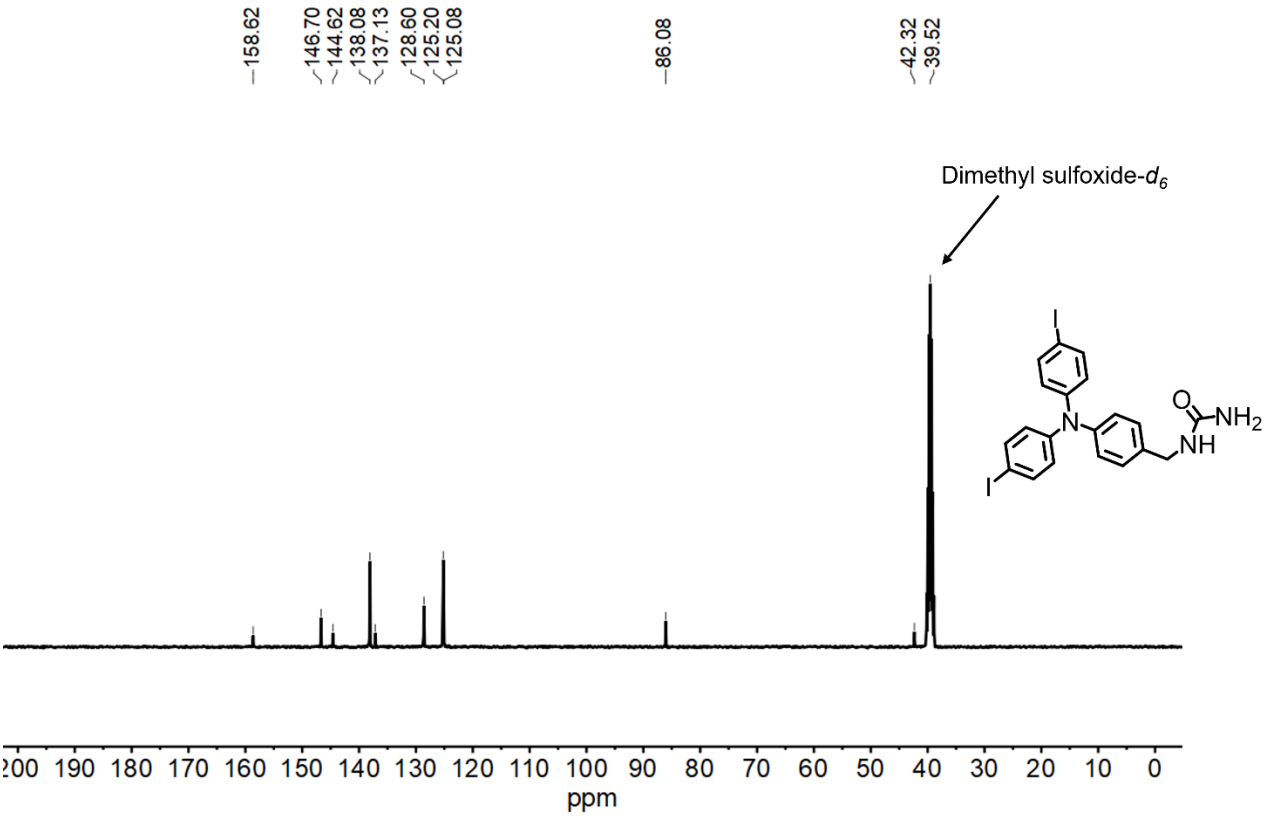

Figure S2. ^{13}C NMR ($(CD_3)_2SO$), 75 MHz)

Synthesis of (4-(bis(4-iodophenyl)amino)phenyl)methanol

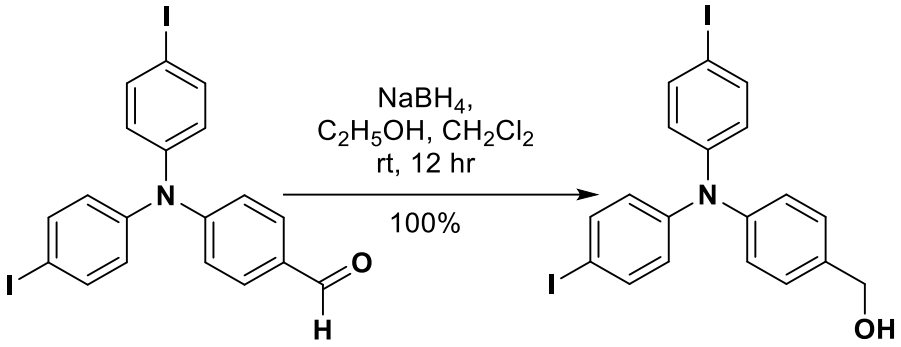

Compound was synthesized according to the previous procedure.[3] Product from the previous step (1.917 g, 3.65 mmol, 1 equiv.) was dissolved in 60 mL of 3:1 mixture of dry CH_2Cl_2 and ethanol and stirred for 5 minutes at room temperature. Then sodium borohydride (0.16 g, 4.01 mmol, 1.1 equiv.) was added to the reaction mixture and stirred for 12 hours at room temperature in the dark. After completion, the reaction mixture was quenched by adding 90 mL of H_2O and the organics were extracted with (3 X 35 mL) CH_2Cl_2 and dried over anhydrous $MgSO_4$. Then the solvent was removed under reduced pressure and the final product was obtained as a sticky white solid (1.921 g, 99 %). The obtained spectra matched with previous reports. ^{1}H NMR (400 MHz, $CDCl_3$) δ(ppm): 7.52 (d, J = 8.8 Hz, 4H), 7.27 (d, J = 7.9 Hz, 2H), 7.05 (d, J = 8.4 Hz, 2H), 6.81 (d, J = 8.8 Hz, 4H), 4.65 (s, 2H).

Synthesis of 4-(bromomethyl)-N,N-bis(4-iodophenyl)aniline

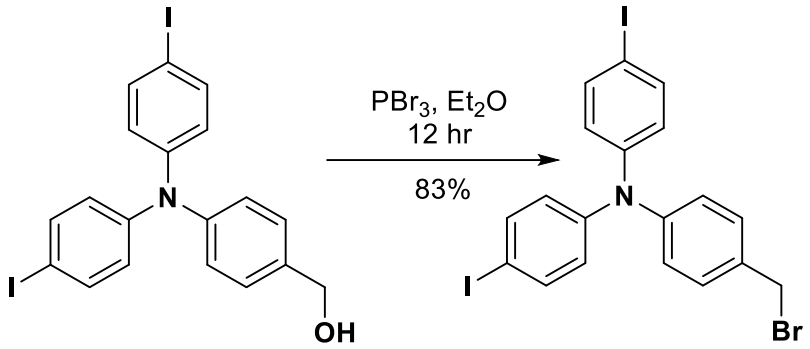

Compound was synthesized according to the previous procedure.[4] The previous alcohol (1.921 g, 3.645 mmol, 1 equiv.) was dissolved in 40 mL of dry diethyl ether and cooled to 0°C in an ice bath. Then phosphorus tribromide (0.652 g, 2.406 mmol, 230 µl, 0.66 equiv.) was added dropwise as a solution in 10 mL dry diethyl ether to the reaction mixture over 5 minutes and stirred at room temperatures in dark for 12 hours. Once finished, 55 mL ice old H_2O and (3 X 20 mL) of saturated $NaHCO_3$ have been added to the reaction mixtures. Then the organics were extracted with (1 x 55 mL) CH_2Cl_2 and further washed with brine (3 x 20 mL) and dried over anhydrous $MgSO_4$. Then the solvent was reduced by using rotary evaporation and the final product was obtained as a sticky solid (2.12 g, 98%). The obtained spectra matched with previous reports. ^{1}H NMR (400 MHz, $CDCl_3$) δ(ppm): 7.54 (d, J = 8.7 Hz, 4H), 7.34 (d, J = 6.4 Hz, 2H), 7.03 (d, J = 8.3 Hz, 2H), 6.79 (d, J = 8.7 Hz, 4H), 4.20 (s, 2H).

Synthesis of 1,3-bis(4-(bis(4-iodophenyl)amino)benzyl)-5-(tert-butyl)-1,3,5-triazinan-2-one

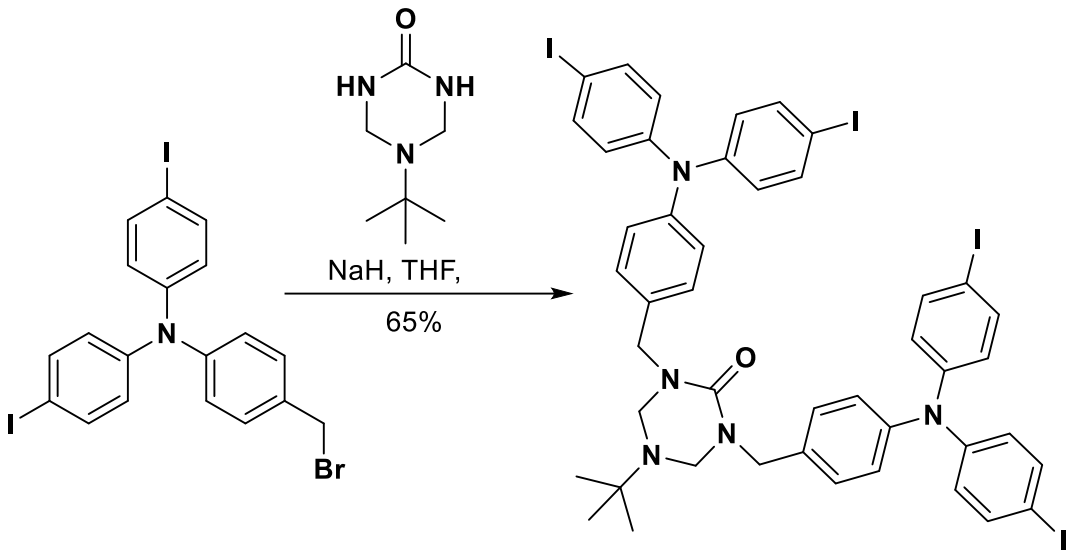

In an oven-dry round bottom flask, 5-(tert-butyl)-1,3,5-triazinan-2-one (0.274 g, 1.74 mmol, 1 equiv.) sodium hydride (0.214 g, 5.34 mmol, 3 equiv.) were added in 27 mL of dry tetrahydrofuran and was stirred for 10 minutes. Then the previous bromide (2.12 g, 3.6 mmol, 2 equiv.) was dissolved in 27 mL of dry tetrahydrofuran and added to the reaction mixtures under the protection of N_2. The reaction mixture was refluxed under the dark for 24 hours. After completion, let the reaction mixture cooled to room temperature and 8 mL of both 1N HCl and H_2O were added to quench the reaction. Then the organics were extracted with (3 x 80 mL) CH_2Cl_2 and washed with brine (1 x 80 mL) and dried over anhydrous $MgSO_4$. Then the solvent was reduced in rotary evaporation and the crude material was further purified by column chromatography using = Hexane: Ethyl Acetate as an eluent. The final product was obtained as a yellow solid (1.370 g, 65%). ^{1}H NMR (300 MHz, (CD3)2CO): δ (ppm) 7.59 (d, J = 8.3 Hz, 8H), 7.37 (d, J = 7.8 Hz, 4H), 7.06 (d, J = 7.8 Hz, 4H), 6.83 (d, J = 8.2 Hz, 8H), 4.51 (s, 4H), 4.33 (s, 4H), 1.00 (s, 9H). ^{13}C NMR (75 MHz, Chloroform-d) δ (ppm) 156.07, 147.03, 145.83, 138.26, 133.81, 129.76, 125.60, 125.04, 85.85, 61.60, 54.41, 48.30, 28.41. HRMS (ES): [M+] calculated 1175.9563; found: 1175.9552.

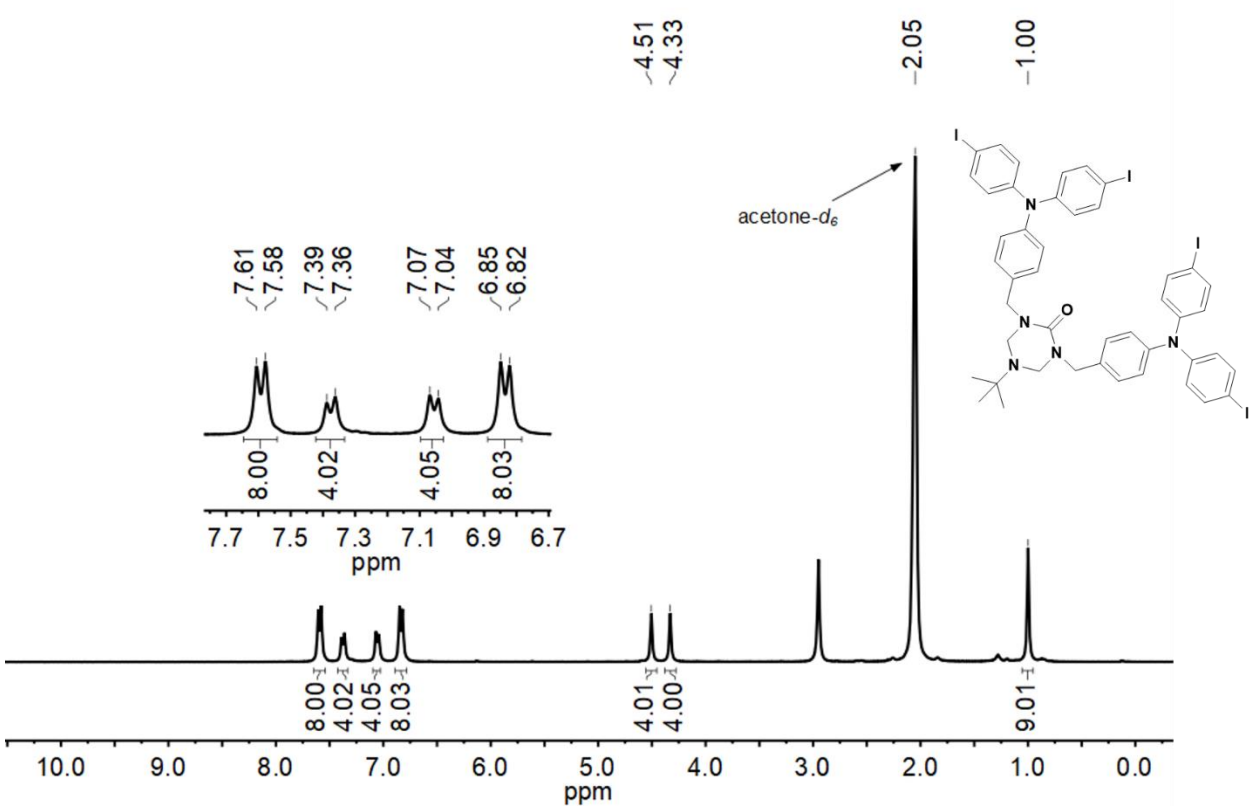

Figure S3. ^{1}H NMR ($(CD_3)_2CO$, 300 MHz)

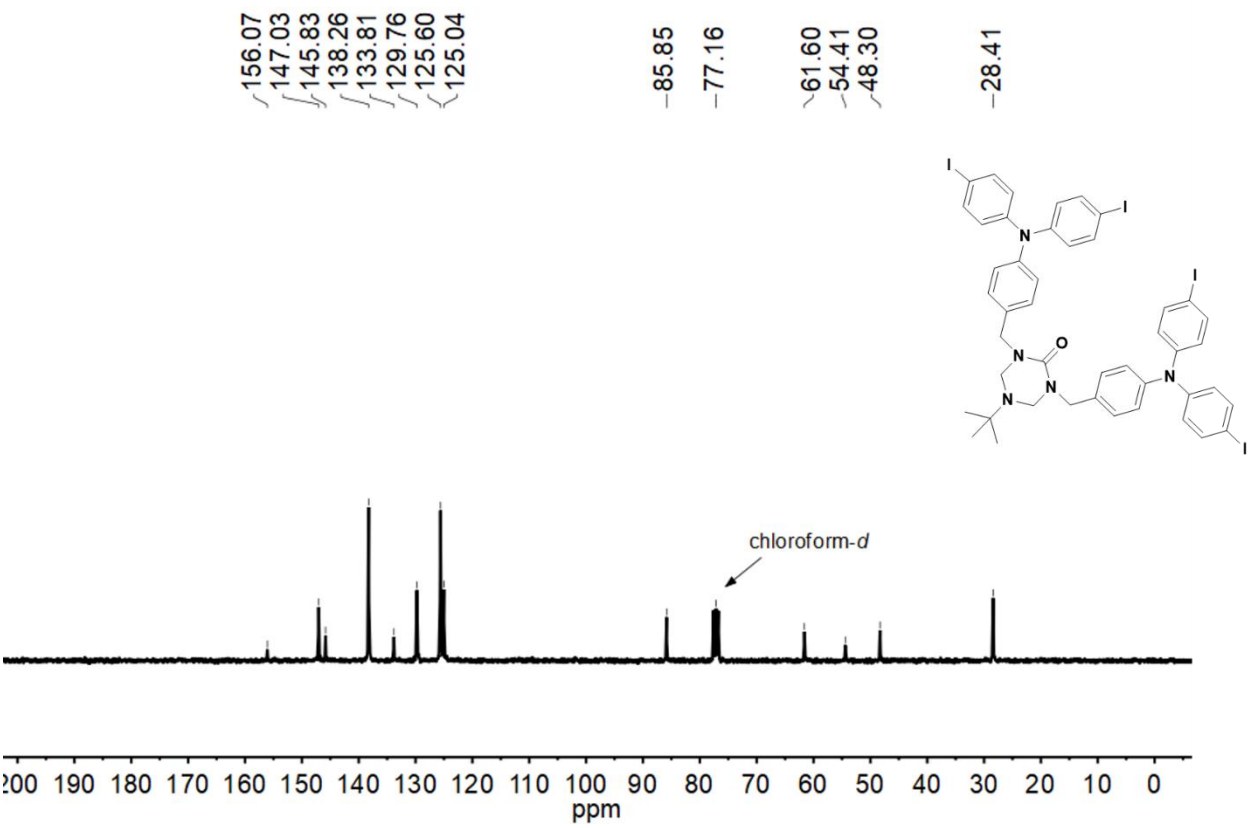

Figure S4. ^{13}C NMR ($CDCl_3$, 75 MHz)

Synthesis of 1,3-bis(4-(bis(4-iodophenyl)amino)benzyl)urea

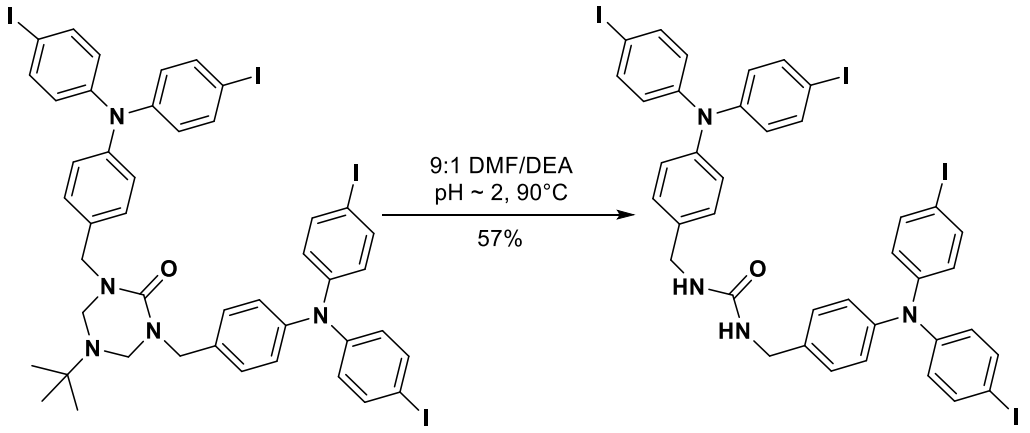

The protected urea from the previous step (0.284 g, 0.241 mmol) was suspended in 134 mL of 9:1 mixture of dimethylformamide and diethanolamine while adjusting the pH at 2 using conc. HCl. Then the reaction was heated at 90°C for 2 days and readjust the pH for every 12 hours interval. After completion, cooled to room temperature, adjust the pH to neutral using $NaHCO_3$ and 200 mL of ice-cold H_2O was added and keep in the refrigerator for 2 hours. Then the precipitant was collected by suction filtration and dried under vacuum. The final product was obtained as a white solid (0.148 g, 57%). ^{1}H NMR (300 MHz, (CD_2Cl_2): δ (ppm) 7.52 (d, *J* = 8.8 Hz, 8H), 7.19 (d, *J* = 8.5 Hz, 4H), 7.01 (d, *J* = 8.5 Hz, 4H), 6.79 (d, *J* = 8.8 Hz, 8H), 4.71 (t, *J* = 5.8 Hz, 2H), 4.33 (d, *J* = 5.9 Hz, 4H). HRMS (ES): [M+] calculated 1078.8671; found: 1078.8672.

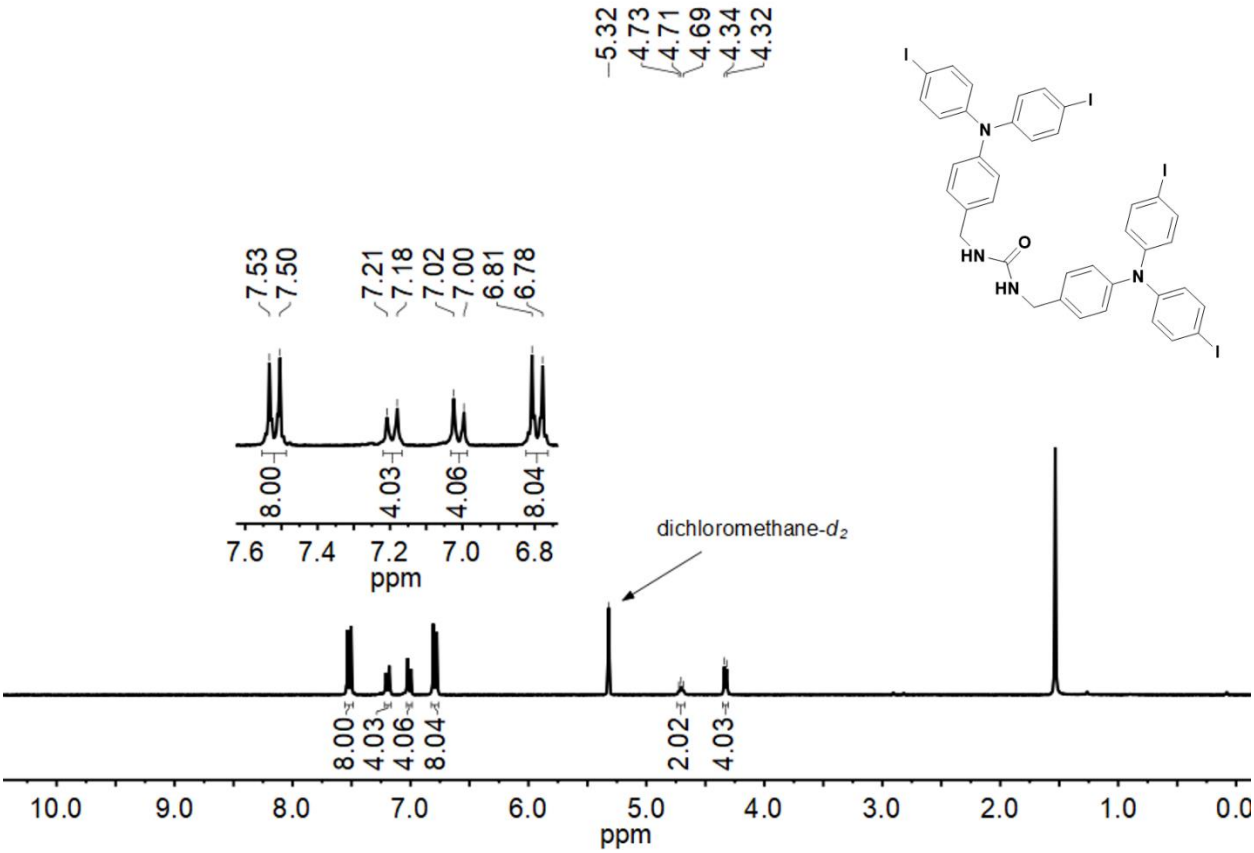

Figure S5. ^{1}H NMR (CD_2Cl_2, 300 MHz)

Crystal data and structure refinement

Single Crystal X-Ray Diffraction (SC-XRD) for Structure Determination, $C_{39}H_{30}I_4N_4O\cdot(C_4H_8O_2)_{0.72(1)}$ (1)

X-ray intensity data from a colorless needle were collected at 100(2) K using a Bruker D8 QUEST diffractometer equipped with a PHOTON-100 CMOS area detector and an Incoatec microfocus source (Mo Kα radiation, λ = 0.71073 Å). The raw area detector data frames were reduced and corrected for absorption effects using the Bruker APEX3, SAINT+ and SADABS programs.[5,6] The structure was solved with SHELXT.[7] Subsequent difference Fourier calculations and full-matrix least-squares refinement against F^2 were performed with SHELXL-2018[7] using OLEX2.[8]

The compound crystallizes in the triclinic system. The space group *P*-1 (No. 2) was confirmed by structure solution. The asymmetric unit consists of half each of two crystallographically independent $C_{39}H_{30}I_4N_4O$ molecules and a region of disordered ethyl acetate (EtOAc) molecules. Both$C_{39}H_{30}I_4N_4O$ molecules are located on crystallographic inversion centers. The central urea group in each is inconsistent with centrosymmetry and is therefore disordered across the inversion center in both independent molecules. Only the urea group atoms are disordered; the remainder of each molecule remains invariant regardless of urea group orientation. The disorder was also observed in the acentric space group *P*1 (No. 1) and therefore is not imposed by incorrectly high space group symmetry. The urea group atoms (O1/N1/N2/C1 and O2/N4/N5/C21) were refined with half-occupancy. Similar C-N distance restraints (SHELX SADI) were applied, and the C=O distances were restrained to 1.20(1) Å. The EtOAc disorder was modeled using three independent molecular components of variable occupancy. All are further disordered about a crystallographic inversion center. Occupancies refined to 0.202(6), 0.269(5) and 0.251(5) for the three components. Appropriate 1,2- and 1,3- C-C and C-O distance restraints (DFIX) were applied to maintain reasonable EtOAc molecular geometries. All EtOAc carbon and oxygen atoms were refined with a common isotropic displacement parameter. All other non-hydrogen atoms were refined with anisotropic displacement parameters. Hydrogen atoms bonded to carbon were located in difference Fourier maps before being placed in geometrically idealized positions and included as riding atoms with *d*(C-H) = 0.95 Å and *U*iso(H) = 1.2*U*eq(C) for aromatic hydrogen atoms, *d*(C-H) = 0.96 Å and *U*iso(H) = 1.2*U*eq(C) for methylene hydrogen atoms and *d*(C-H) = 0.98 Å and *U*iso(H) = 1.5*U*eq(C) for methyl hydrogens. The largest residual electron density peak in the final difference map is 0.84 $e^-/Å^3$, located 0.92 Å from I2.

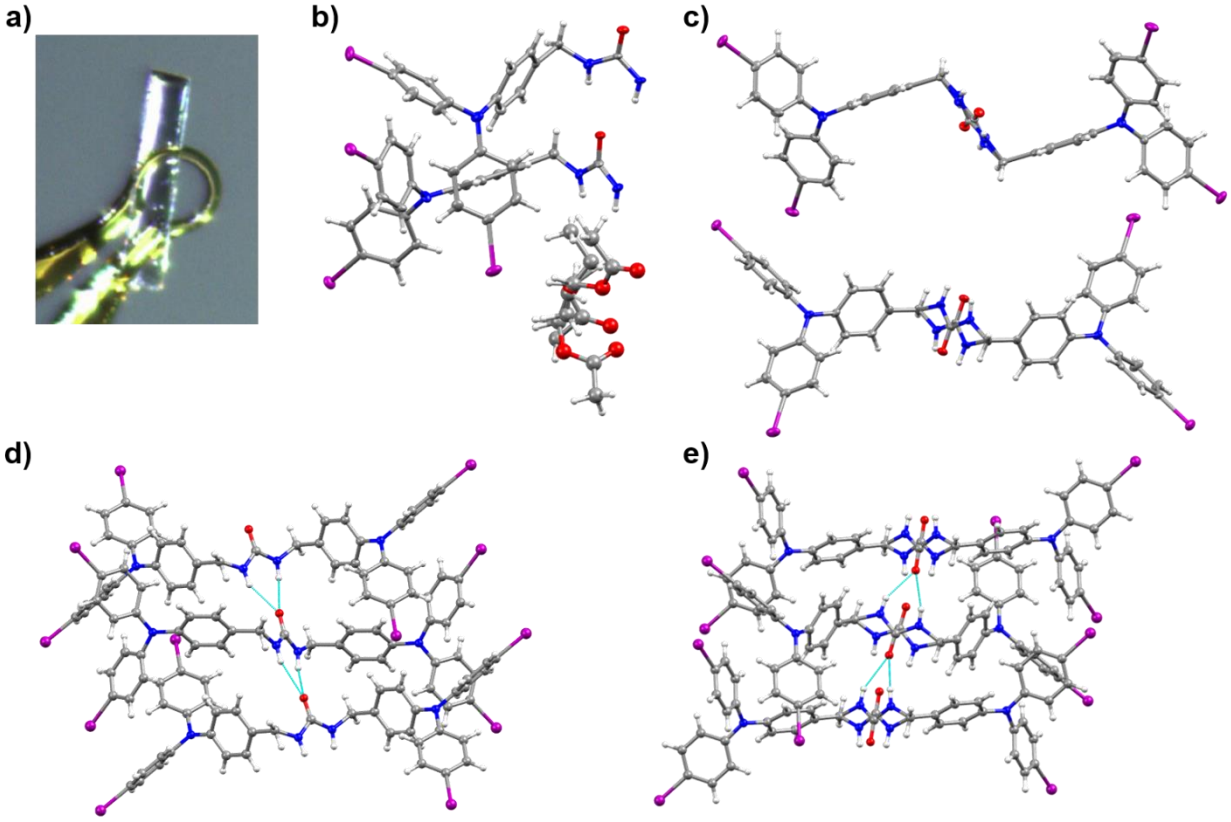

Figure S6. a) Data crystal **1** (ethyl acetate solvated) b) Asymmetric unit of the crystal. Displacement ellipsoid drawn at the 50% probability level. c) The urea group in each independent molecule is disordered across an inversion center. Each urea component is 50% occupied. Displacement ellipsoids drawn at the 50% probability level. d) Disorder model. Crystal consists of 50/50 disorder of chains with urea groups pointing “up” e) chains with urea groups pointing “down”. The average throughout the crystal of the two is shown in the right image. Only the urea group atoms are affected; the remaining atoms of each molecule are common to the two urea components.

Single Crystal X-Ray Diffraction (SC-XRD) for Structure Determination, $C_{39}H_{30}I_4N_4O \cdot 2(CH_3OH)$ (1)

X-ray intensity data from a colorless plate were collected at 100(2) K using a Bruker D8 QUEST diffractometer equipped with a PHOTON-100 CMOS area detector and an Incoatec microfocus source (Mo Kα radiation, λ = 0.71073 Å). The raw area detector data frames were reduced and corrected for absorption effects using the Bruker APEX3, SAINT+ and SADABS programs.[5,6] The structure was solved with SHELXT.[7] Subsequent difference Fourier calculations and full-matrix least-squares refinement against F^2 were performed with SHELXL-2018[7] using OLEX2.[8]

The compound crystallizes in the triclinic system. The space group *P*-1 (No. 2) was confirmed by structure solution. The asymmetric unit consists of half each of two crystallographically independent $C_{39}H_{30}I_4N_4O$ molecules and a region of severely disordered molecules which were modeled as methanol. Both $C_{39}H_{30}I_4N_4O$ molecules are located on crystallographic inversion centers. The central urea group in each is inconsistent with centrosymmetry and is therefore disordered across the inversion center in both independent molecules. Only the urea group atoms are disordered; the remainder of each molecule remains invariant regardless of urea group orientation. The disorder was also observed in the acentric space group *P*1 (No. 1) and therefore is not imposed by incorrectly high space group symmetry. The urea group atoms (O1/N1/N2/C1 and O2/N4/N5/C21) were refined with half-occupancy. Similar C-N distance restraints (SHELX SADI) were applied, and the C=O distances were restrained to 1.20(1) Å. The methanol disorder was modeled using seven independent components of variable occupancy. Refined occupancies ranged from C1S/O1S = 0.460(9) to C7S/O7S = 0.16(1). Constraints were applied such that the sum of atomic occupancies of independent disorder components within van der Waals radii of each other was less than one. Methanol C-O distances were restrained to 1.45(1) Å using DFIX instructions. All methanol carbon and oxygen atoms were refined with a common isotropic displacement parameter. All other non-hydrogen atoms were refined with anisotropic displacement parameters. Hydrogen atoms bonded to carbon were located in difference Fourier maps before being placed in geometrically idealized positions and included as riding atoms with *d*(C-H) = 0.95 Å and *U*iso(H) = 1.2*U*eq(C) for aromatic hydrogen atoms and *d*(C-H) = 0.96 Å and *U*iso(H) = 1.2*U*eq(C) for methylene hydrogen atoms. No hydrogen atoms were located or calculated for the methanol species. The largest residual electron density peak in the final difference map is 1.01 $e^-/Å^3$, located 0.71 Å from I2.

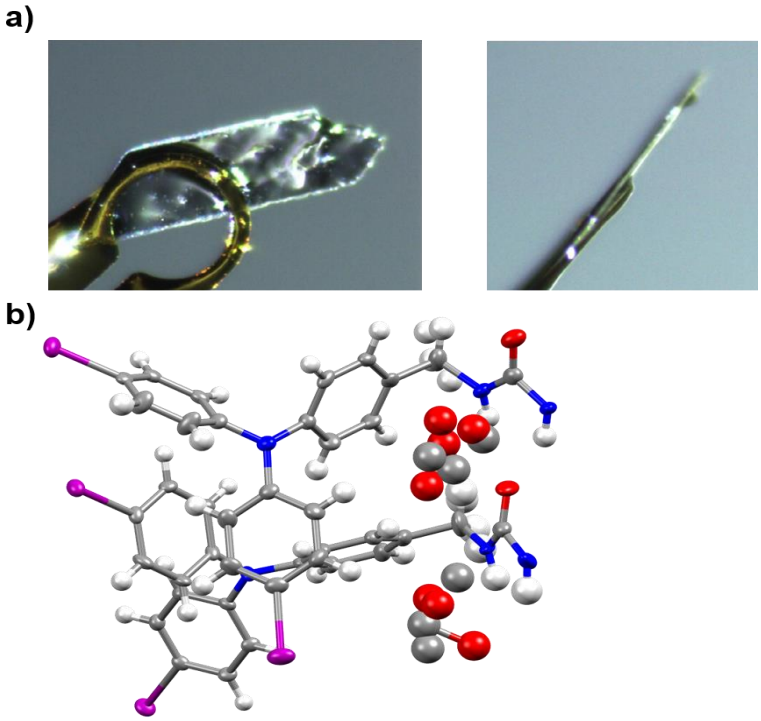

Figure S7. a) Data crystal **1** (methanol solvated). b) Asymmetric unit of the crystal. Displacement ellipsoid drawn at the 50% probability level.

X-Ray Structure Determination, $C_{20}H_{17}I_2N_3O$ (2)

X-ray intensity data from a colorless plate were collected at 100(2) K using a Bruker D8 QUEST diffractometer equipped with a PHOTON-II area detector and an Incoatec microfocus source (Mo Kα radiation, λ = 0.71073 Å). The raw area detector data frames were reduced, scaled and corrected for absorption effects using the Bruker APEX3, SAINT+ and SADABS programs.[5,6] The structure was solved with SHELXT. Subsequent difference Fourier calculations and full-matrix least-squares refinement against F^2 were performed with SHELXL-2018[7] using OLEX2.[8]

The compound crystallizes in the triclinic system. The space group *P*-1 (No. 2) was confirmed by structure solution. The asymmetric unit consists of two crystallographically independent but chemically identical molecules. All non-hydrogen atoms were refined with anisotropic displacement parameters. All hydrogen atoms were located in difference Fourier maps. Those bonded to carbon were placed in geometrically idealized positions and included as riding atoms with *d*(C-H) = 0.95 Å and *U*iso(H) = 1.2*U*eq(C) for arene hydrogen atoms and *d*(C-H) = 0.99 Å and *U*iso(H) = 1.2*U*eq(C) for methylene hydrogen atoms. Hydrogen atoms bonded to nitrogen were located and refined isotropically with *d*(N-H) = 0.86 Å distance restraints. The largest residual electron density peak in the final difference map is 0.95 $e^-/Å^3$, located 0.73 Å from I1.

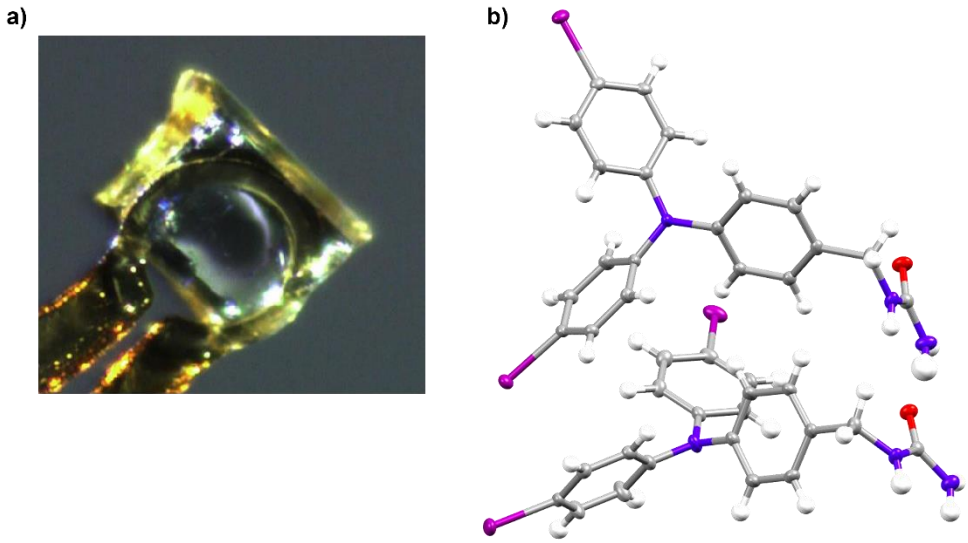

Figure S8. a) Data crystal **2**. b) Asymmetric unit of the crystal. Displacement ellipsoids drawn at the 50% probability level. Twin crystallographically independent but chemically identical molecules.

Single Crystal X-Ray Diffraction (SC-XRD) for Structure Determination, $C_{19}H_{13}I_2NO$ (3)

X-ray intensity data from a pale yellow plate were collected at 100(2) K using a Bruker D8 QUEST diffractometer equipped with a PHOTON-II area detector and an Incoatec microfocus source (Mo Kα radiation, λ = 0.71073 Å). The raw area detector data frames were reduced, scaled and corrected for absorption effects using the Bruker APEX3, SAINT+ and SADABS programs.[5,6] The structure was solved with SHELXT.[7] Subsequent difference Fourier calculations and full-matrix least-squares refinement against F^2 were performed with SHELXL-2018[7] using OLEX2.[8]

The compound crystallizes in the monoclinic system. The pattern of systematic absences in the intensity data was consistent with the space groups *Pc* and *P*2/*c*. The acentric group *Pc* was found by the solution program XT, and was confirmed by obtaining a reasonable and stable structural model. The space group choice was further verified with ADDSYM, which found no missed symmetry elements. A hypothetical non-disordered structure was used to enable the ADDSYM search. The asymmetric unit in *Pc* consists of one molecule. The structure is disordered, with the formyl group and iodine ligands I2 and I3 scrambled together on two separate sites. This was identified by observation of abnormally large iodine displacement parameters when I2 and I3 were refined with full occupancies, and also by difficulty in locating the formyl group atoms. Trial refinements of the I2 and I3 occupancies resulted in significant reduction from 100% along with a large decrease in *R*-values. Subsequently, difference Fourier peaks corresponding to formyl group carbon and oxygen atoms were observed near the partially occupied I2 and I3 sites. The formyl group scrambled with I3 is further disordered over two orientations C20A/O2A and C20B/O2B. The occupancy of iodine site I1 refined to 100% iodine, and is not disordered with a formyl group. For the final cycles, *d*(C-C) = 1.47(2) Å and *d*(C-O) = 1.25(2) Å distance restraints were used. The disorder fractions at each substituent site refined to: I2/C19-O1 = 0.745(2)/0.255(2) and I3/C20A-O20A/C20B-O20B = 0.256(2)/0.342(3)/0.402(3). All non-hydrogen atoms were refined with anisotropic displacement parameters except for the disordered formyl group atoms (isotropic). Hydrogen atoms bonded to carbon were in general located in difference Fourier maps before being placed in geometrically idealized positions and included as riding atoms with *d*(C-H) = 0.95 Å and *U*iso(H) = 1.2*U*eq(C). The largest residual electron density peak in the final difference map is 0.94 $e^-/Å^3$, located 0.45 Å from H19. The absolute structure (Flack) parameter after the final refinement cycle was 0.019(11).

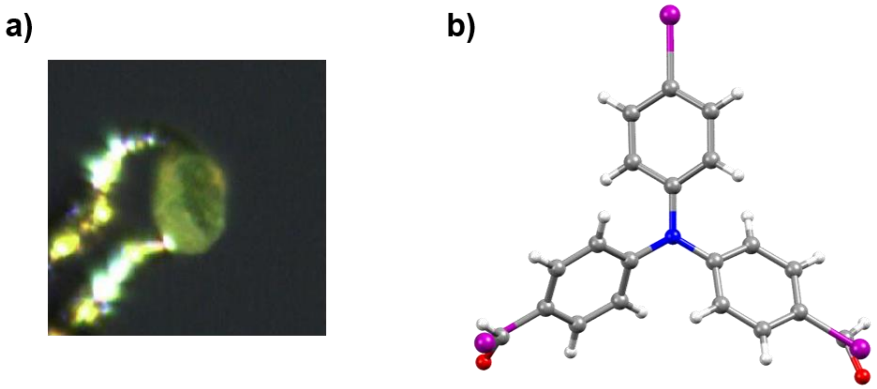

Figure S9. (a) Data Crystal **3**. (b) disordered with the formyl group and iodines scrambled together on two separate sites.

Table S1. X-ray structure refinement data

Empirical formula	$C_{41.89}H_{35.78}I_4N_4O_{2.44}$	$C_{41}H_{30}I_4N_4O_3$	$C_{20}H_{17}I_2N_3O$	$C_{19}H_{13}I_2NO$
CCDC	2165901	2165898	2165899	2165900
Formula weight	1141.92	1134.29	569.17	525.10
Temperature/K	100(2)	100(2)	100(2)	100(2)
Crystal system	triclinic	triclinic	triclinic	monoclinic
Space group	P-1	P-1	P-1	Pc
a/Å	9.5202(4)	9.4847(12)	9.4579(4)	9.7182(3)
b/Å	10.0356(4)	9.8569(13)	9.9193(4)	8.0639(2)
c/Å	23.9703(9)	23.787(3)	23.4761(9)	11.5611(3)
α/°	92.092(2)	91.327(3)	90.9100(10)	90
β/°	100.214(2)	100.187(3)	99.539(2)	107.3914(9)
γ/°	114.586(2)	114.405(3)	114.9540(10)	90
Volume/$Å^3$	2033.89(14)	1981.7(4)	1960.13(14)	864.59(4)
Z	2	2	4	2
$\rho_{calc}g/cm^3$	1.865	1.901	1.929	2.017
μ/mm^{-1}	3.106	3.188	3.223	3.641
F(000)	1093.0	1080.0	1088.0	496.0
Crystal size/mm^3	0.34 × 0.06 × 0.02	0.54 × 0.22 × 0.02	0.3 × 0.22 × 0.12	0.12 × 0.07 × 0.05
Radiation	MoKα (λ = 0.71073)	MoKα (λ = 0.71073)	MoKα (λ = 0.71073)	MoKα (λ = 0.71073)
2Θ range for data collection/°	4.498 to 52.798	4.564 to 53.404	4.55 to 66.376	4.392 to 56.576
Index ranges	-11 ≤ h ≤ 11, -12 ≤ k ≤ 11, -29 ≤ l ≤ 29	-11 ≤ h ≤ 11, -12 ≤ k ≤ 12, -29 ≤ l ≤ 30	-14 ≤ h ≤ 14, -15 ≤ k ≤ 15, -36 ≤ l ≤ 36	-12 ≤ h ≤ 12, -10 ≤ k ≤ 10, -15 ≤ l ≤ 15
Reflections collected	46016	39928	76938	24434
Independent reflections	8313 [R_{int} = 0.0452, R_{sigma} = 0.0303]	8311 [R_{int} = 0.0637, R_{sigma} = 0.0474]	14982 [R_{int} = 0.0437, R_{sigma} = 0.0358]	4193 [R_{int} = 0.0280, R_{sigma} = 0.0213]
Data/restraints/parameters	8313/50/528	8311/35/517	14982/6/494	4193/11/225
Goodness-of-fit on F^2	1.242	1.035	1.021	1.160

Final R indexes [I>=2σ (I)]	R_1 = 0.0362, wR_2 = 0.0745	R_1 = 0.0373, wR_2 = 0.0721	R1 = 0.0275, wR2 = 0.0512	R1 = 0.0275, wR2 = 0.0644
Final R indexes [all data]	R_1 = 0.0455, wR_2 = 0.0771	R_1 = 0.0610, wR_2 = 0.0818	R1 = 0.0442, wR2 = 0.0553	R1 = 0.0296, wR2 = 0.0662
Largest diff. peak/hole / e $Å^{-3}$	0.83/-0.68	1.01/-1.03	0.95/-1.08	0.95/-0.76

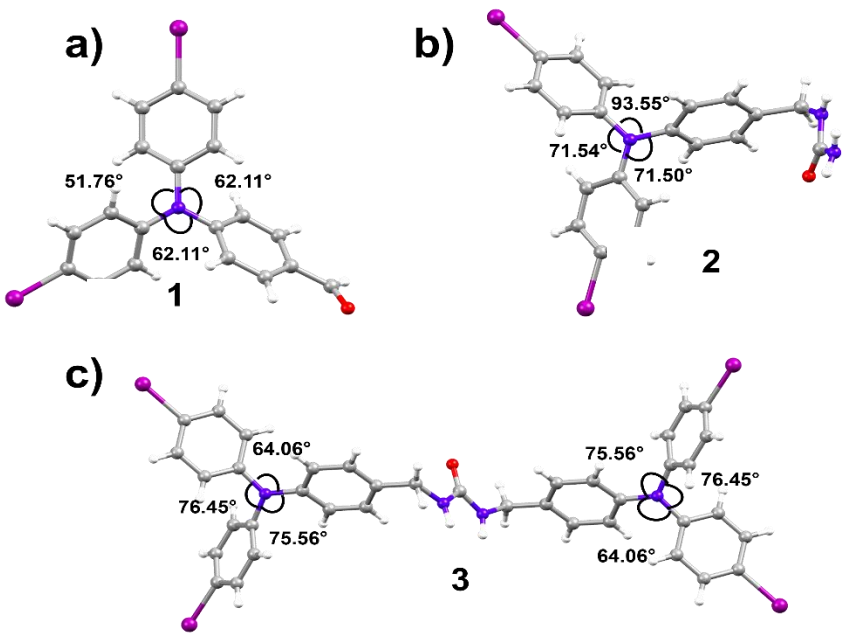

Figure S10. Structure and orientation of TPA unit. a) propeller conformations of TPA unit for **3**. b) propeller conformations of TPA unit for **2**. C) chiral propeller conformation of TPA unit for **1**. Symmetric orientation observed on both side of the TPA units.

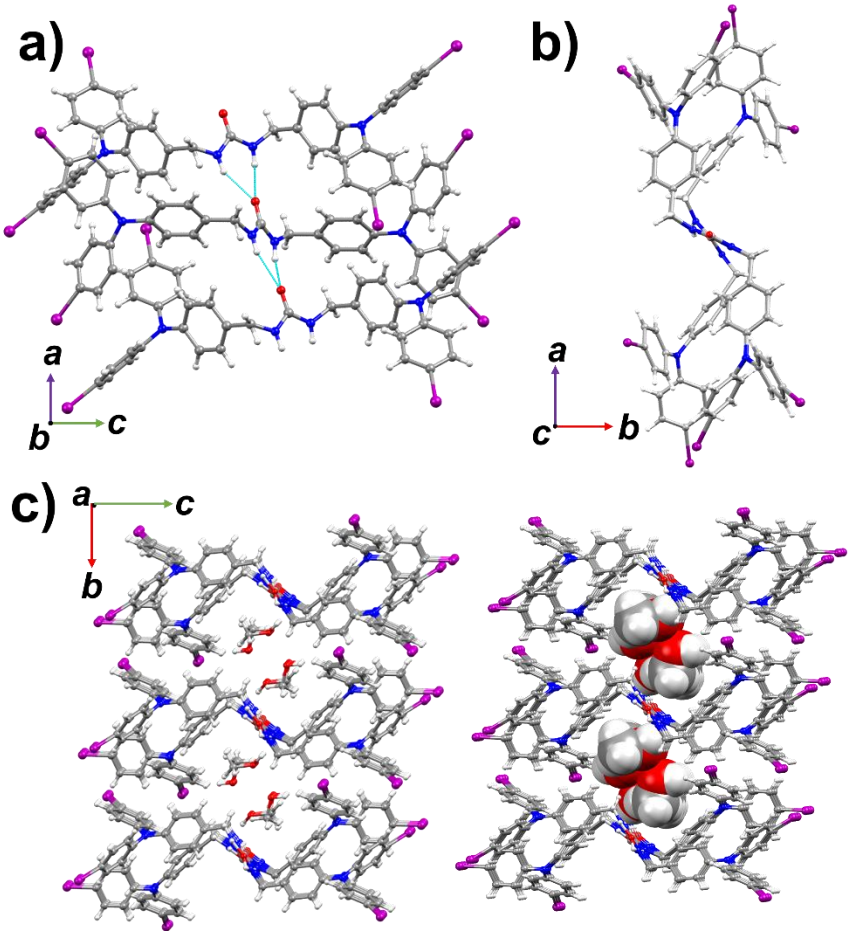

Figure S11. Comparison of urea tethered solvated crystal of **1**. a) side view of crystal **1** showing hydrogen bonded urea tape. b) urea chains formed a skewed shape if viewed along crystallographic *c* – axis. c) H-bonded urea chains encapsulate solvent (methanol shown left). Methanol solvent in spacefill model (right).

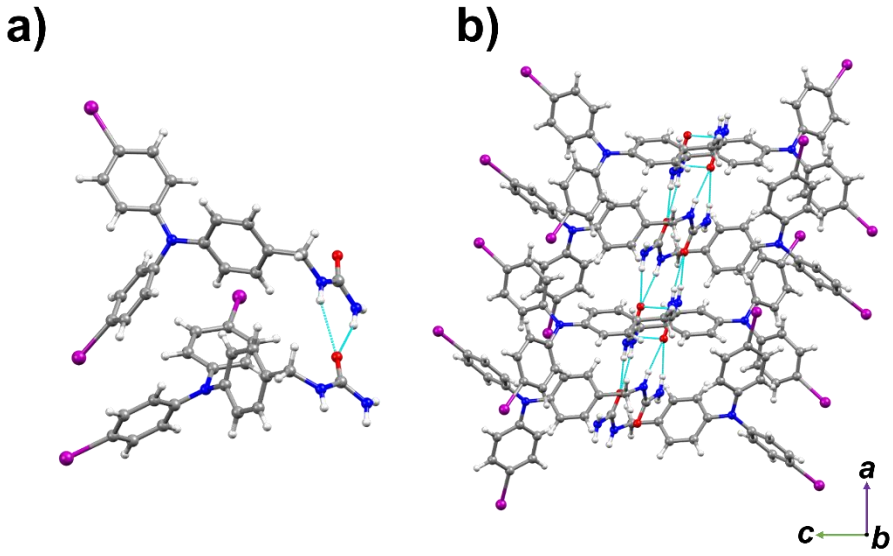

Figure S12. Views of X-ray structure of **2**. a) assembly through hydrogen bonded urea tape. b) inter-chain H-bonds links two strands (side view).

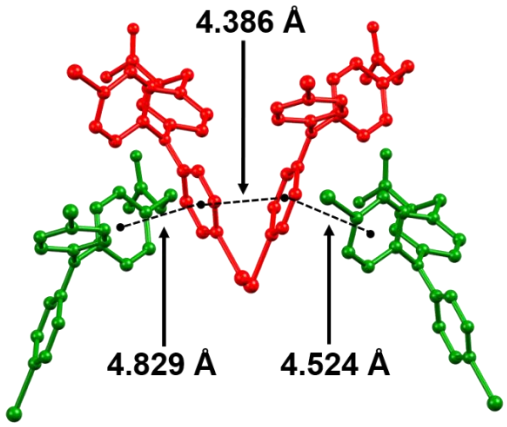

Figure S13. Views of packed **1** showing face-to-face π-stacking metrics between different TPA units. Distances were measured between phenyl ring centroids. Symmetry equivalent TPA units are colored either red or green. Guest molecules, hydrogen atoms, and non-relevant parts of the structure were removed for clarity.

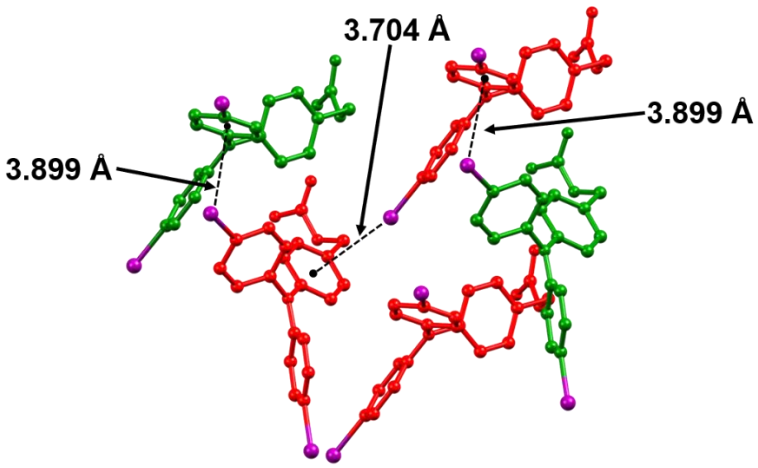

Figure S14. Views of packed **1** showing halogen C-I···π interactions between different TPA units. Distances were measured from the phenyl ring centroids to the covalently bonded iodine. Symmetry equivalent TPA units either colored red or green. Guest molecules, hydrogen atoms, and non-relevant parts of the structure were removed for clarity.

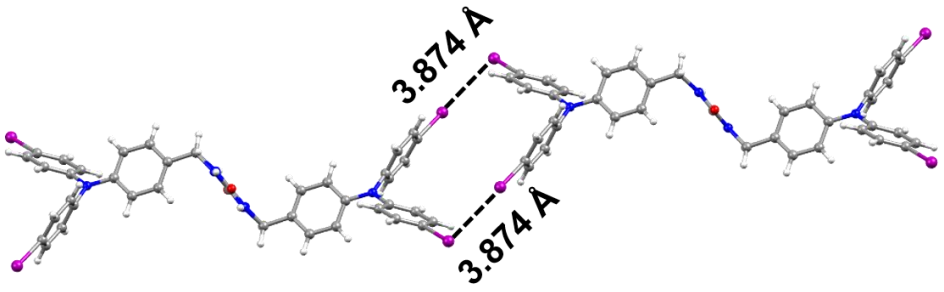

Figure S15. Views of packed **1** showing an I···I interaction (halogen bond) with neighbouring TPA. The I···I distance of 3.874 Å less than sum of iodine van der Waals radii (3.96 Å). This halogen bond assists in holding the column together.

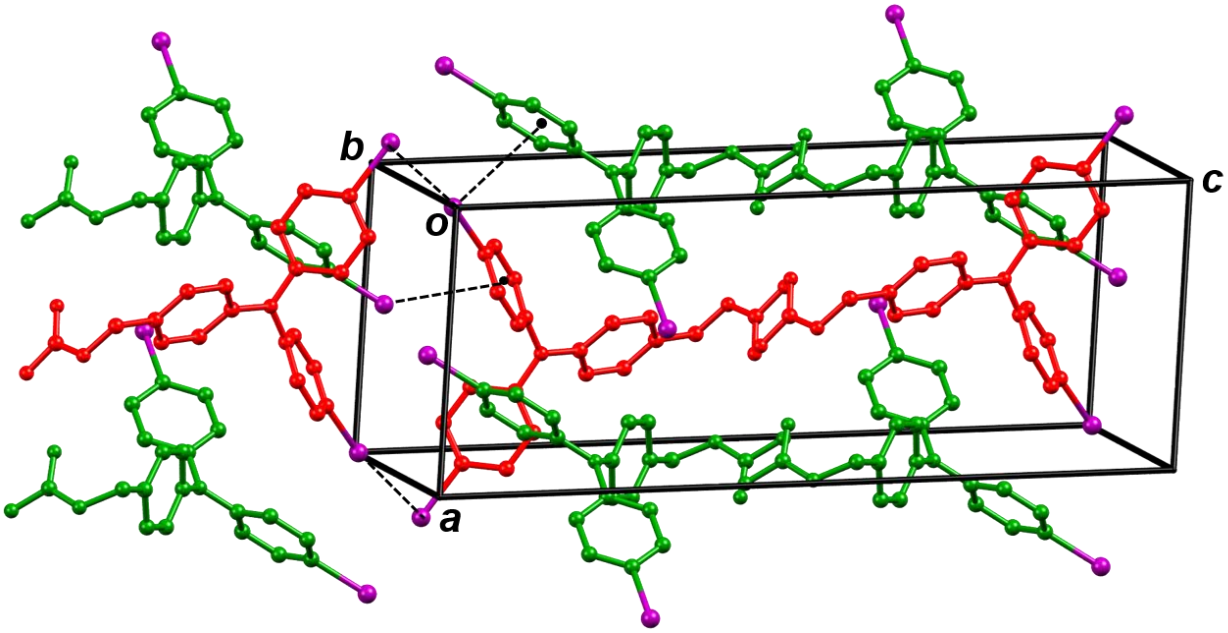

Figure S16. Unit cell of **2**. Symmetry equivalent TPA units either colored red or green.

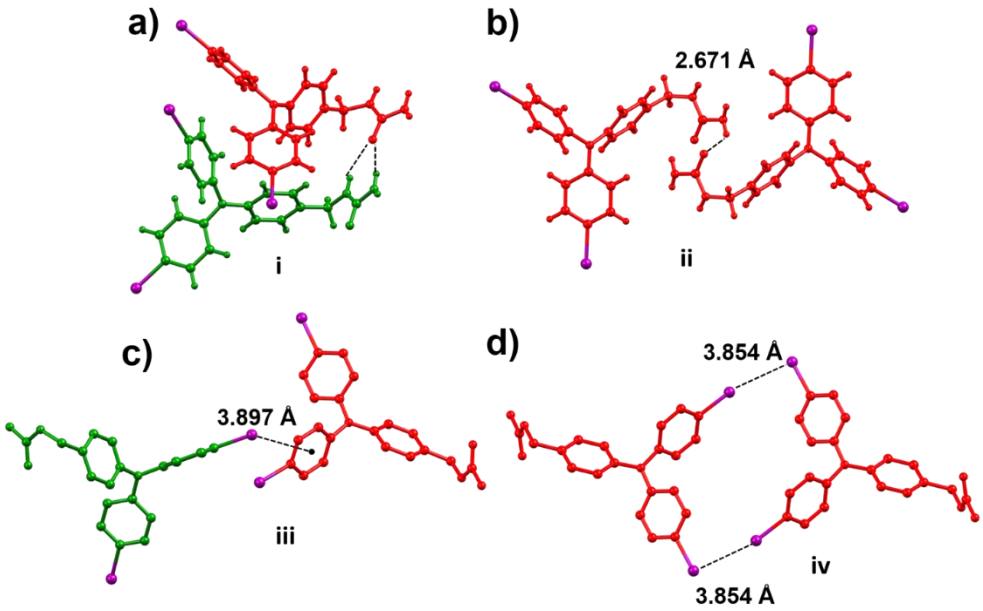

Figure S17. Dimer model of **2**. Symmetry equivalent TPA units either colored red or green.

Table S2. Measured photophysical properties for compounds **1**, **2**, and **3**.

Compound	λ_{abs} (nm)[a]	λ_{ems} (nm)[b]
3 in solid	445	478
2 in solid	367	503
1 in solid	361	451
1 (in Methylene chloride)	309	365, 440
1 (in thin films)	321	

[a]Peak position at the largest absorption band. In solid diffuse reflectance experiments performed in bulk crystals. [b]Peak position at the largest emission bands in nanometers using 375 nm laser excitation source for solid and 300 nm excitation source for solution (10 μM) and in thin films. In solid, photoluminescence experiments performed in single crystals.

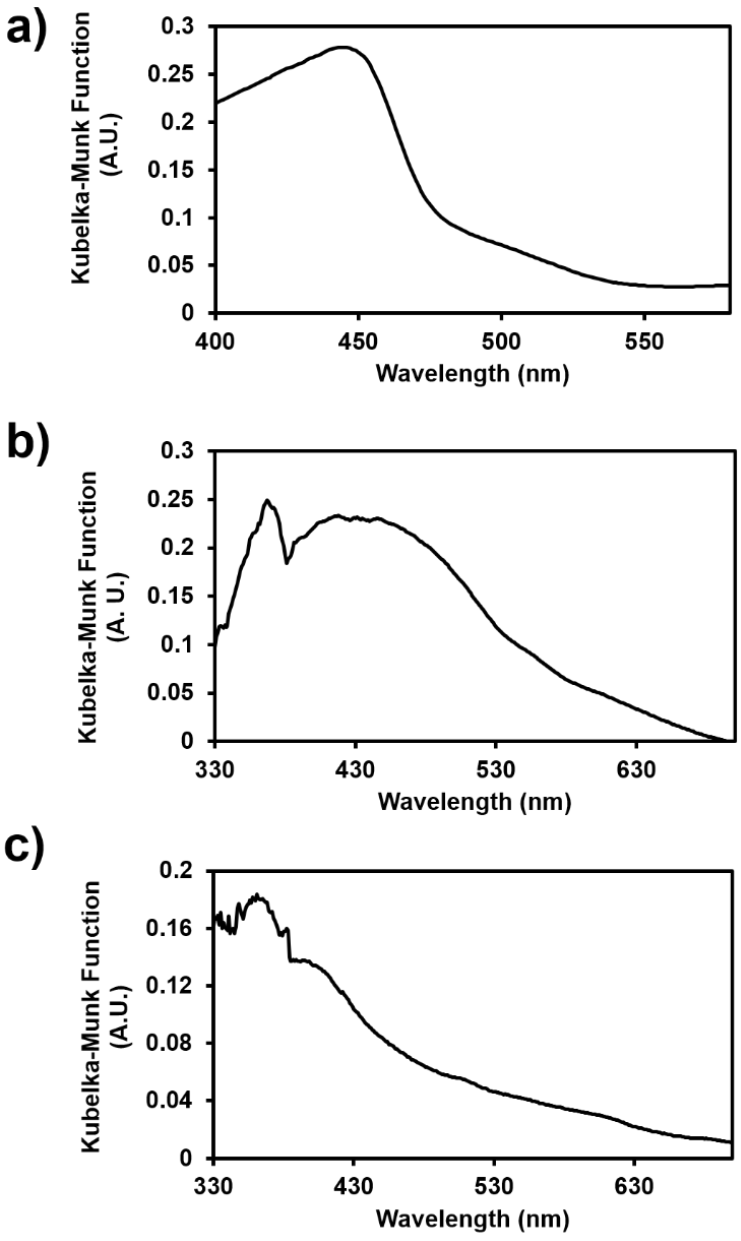

Figure S18. Diffuse reflectance experiments performed in bulk crystals. a) Diffuse reflectance spectra of **3**. b) Diffuse reflectance spectra of **2**. c) Diffuse reflectance spectra of **1**.

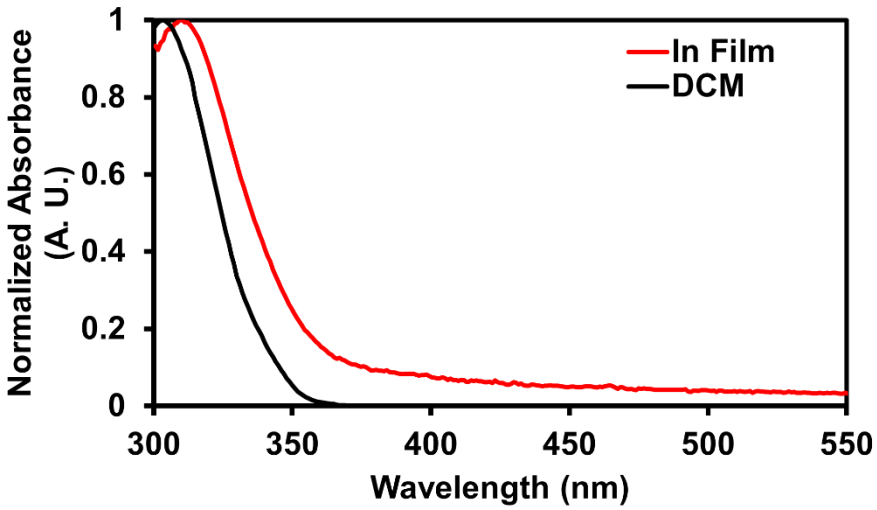

Figure S19. UV-vis absorption spectrum of **1** in dry methylene chloride (10 µm) (inset black) and in thin film (inset red).

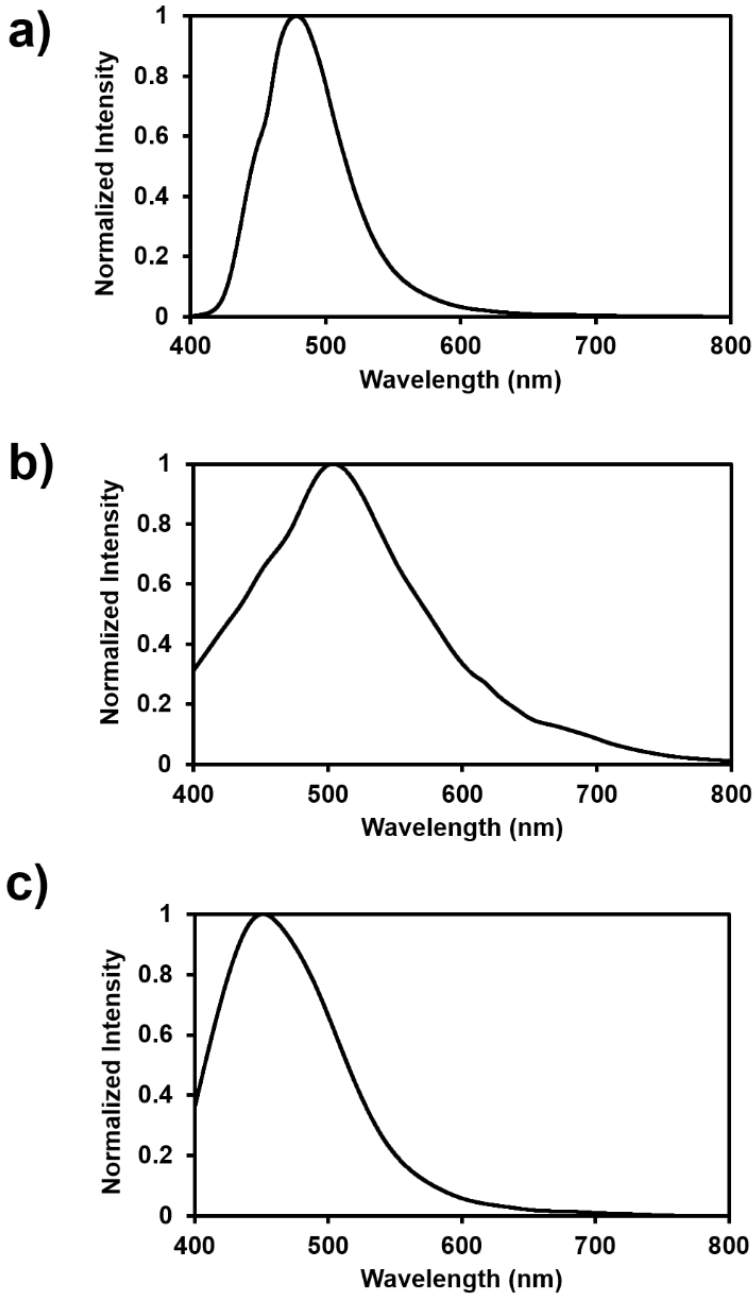

Figure S20. Normalized emission spectra of single crystal for compound (a) **3**, (b) **2**, (c) **1**. For excitation 375 nm laser source were used.

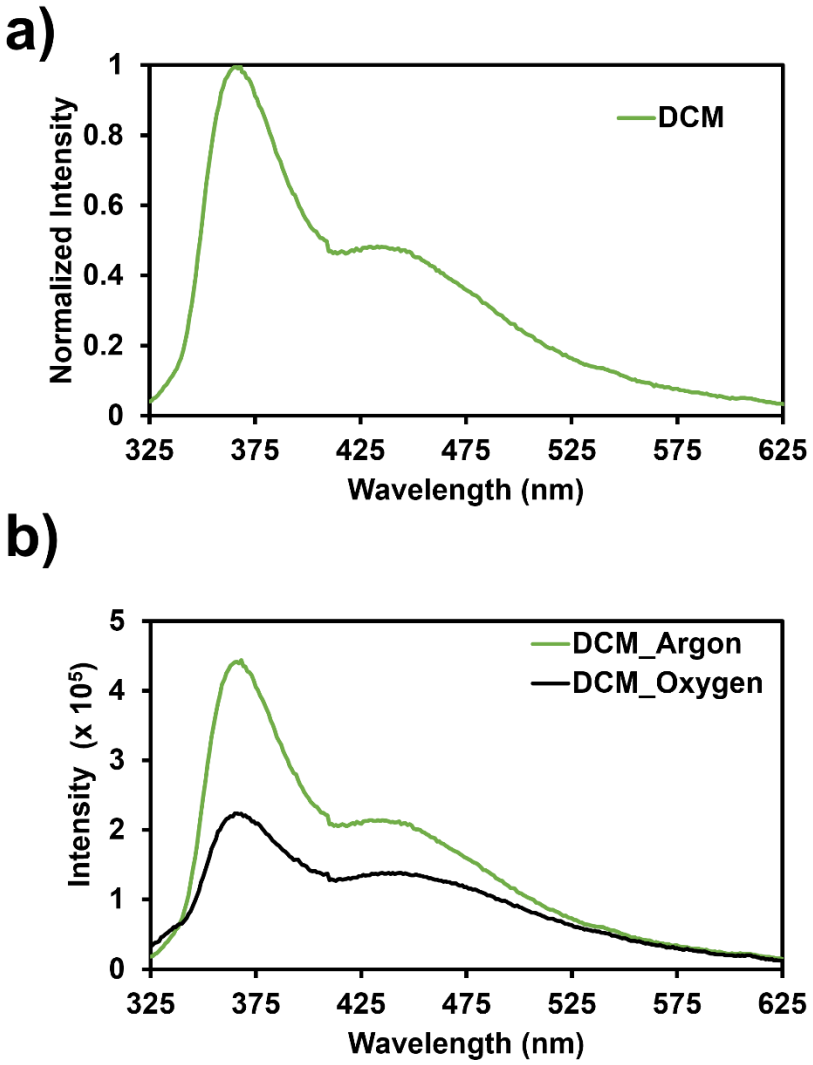

Figure S21. UV-vis emission spectrum of **1** in methylene chloride using 300 nm excitation source. a) UV-vis emission spectrum of 1 in dry methylene chloride (10 µM). b) comparison of UV-vis emission spectrum of **1** in dry CH_2Cl_2 (10 µM). (argon purged, inset green) and in CH_2Cl_2 (10 µM) (oxygen purged, inset black).

Conductivity Experiments in Single Crystal

A single crystal was placed on a PMMA coated SiO2/Si substrate. Gold contacts were deposited through e-beam evaporation, using a shadow mask technique. Contact regions were defined using a slotted metal shadow mask together with a gold wire, carefully aligned perpendicular to the crystal, to define a narrow gap between contact regions covering each end of the crystal. A 100 nm thick gold top contact was deposited at a rate of 2 Å/s. Finally, the gold wire and shadow mask were removed, and the device was measured for electrical conductance. There was negligible current while parking the probes on the surrounding gold pads, as the gold film on top of the crystals was not continuous with them due to the thickness of the crystals. However, a significant current was observed when probes were placed on the metal films on top of the crystals. Measurements were performed in the dark, at room temperature.

As an example of conductivity measure in a single crystal of **1**
Sample height (thickness) estimated through focusing stage 0.001" = 25.4 µm
Length estimated at 100x resolution = 25 µm
width estimated at 100x resolution = 77 µm
Current 1.1×10^{-10} Amps at 10 V bias

$$\rho = R.\frac{A}{L} = \frac{V}{I}.\frac{A}{L}$$

$$\rho=(10/1.1\times10^{-10}) \text{ x } (77 \times 10^{-6} \text{ x } 25.4\times10^{-6} / 25\times10^{-6})$$

$$\rho = 7112000\ \Omega m = 711200000\ \Omega.cm$$

$$\text{Conductivity} = 1.41 \text{ x } 10^{-9}\ S\cdot cm^{-1}$$

Table S3. Conductivity measurement of the single crystal **2**.

Trials #	σ (S·cm^{-1})	Length (μm)	Width (μm)	Thickness (μm)
1	6.44 x 10^{-7}	94	239.361	50.8
2	5.40 x 10^{-7}	25	186.16	76
3	2.93 x 10^{-10}	25	405.92	10

Table S4. Conductivity measurement of the single crystal **1**.

Trials #	σ (S·cm^{-1})	Length (μm)	Width (μm)	Thickness (μm)
1	1.41 x 10^{-9}	25	77	25.4
2	1.77 x 10^{-8}	25	72.48	5
3	1.65 x 10^{-8}	25	75.92	5

Table S5. Conductivity measurement of the single crystal **1** at time interval upon UV irradiation using 365 nm light source.

Time (hr)	σ (S·cm^{-1})
0	1.65 x 10^{-8}
0.25	1.36 x 10^{-8}
1	9.29 x 10^{-9}
1.5	8.65 x 10^{-9}
2	7.73 x 10^{-9}
3	6.95 x 10^{-9}
4	5.81 x 10^{-9}
5	5.12 x 10^{-9}

Table S6. Conductivity measurement of the single crystal of **2** at time interval upon UV irradiation using 365 nm light source

Time (hr)	σ (S·cm^{-1})
0	5.39 x 10^{-7}
0.25	4.00 x 10^{-7}
0.5	3.86 x 10^{-7}
0.75	3.85 x 10^{-7}
1	3.80 x 10^{-7}
2	3.74 x 10^{-7}
3	3.62 x 10^{-7}
4	3.58 x 10^{-7}
5	3.60 x 10^{-7}

Table S7. Conductivity measurement of the single crystal of **1** in dark after 5 hours of UV irradiation

Time (hr)	σ (S·cm^{-1})
0	5.12 x 10^{-9}
0.25	5.99 x 10^{-9}
0.5	6.16 x 10^{-9}
0.75	6.16 x 10^{-9}
1	6.16 x 10^{-9}
2	5.92 x 10^{-9}

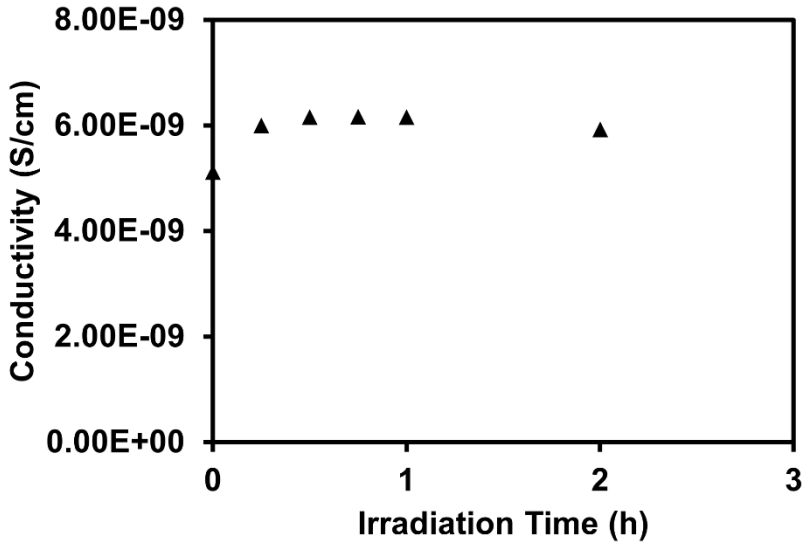

Figure S22. Electrical conductivity measurement at time interval in dark at room temperature of single crystals of **1** after 5 hours of UV irradiation

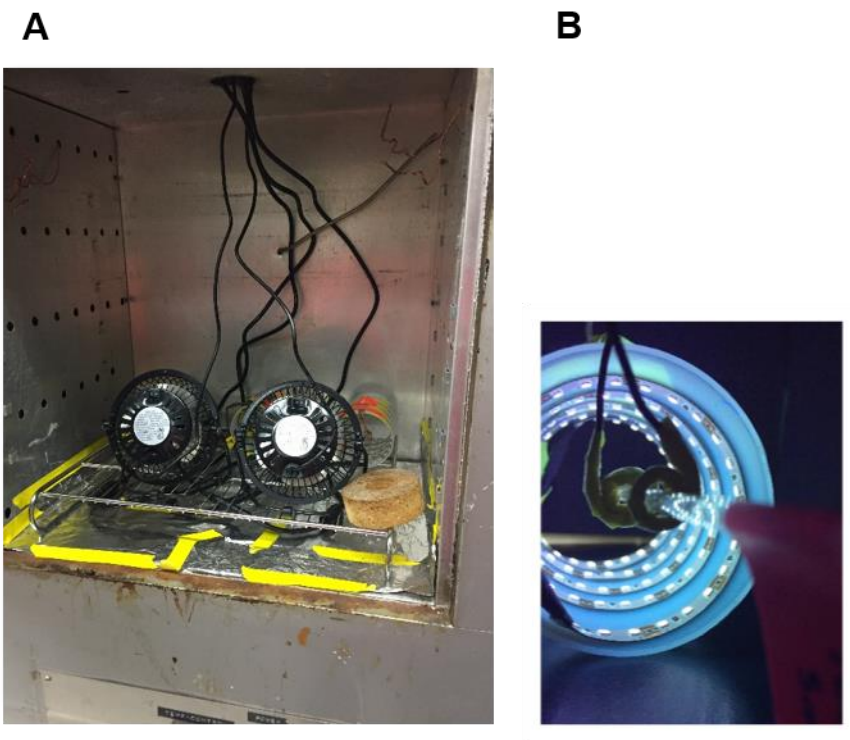

Figure S23. Photoreactor used in maximum radical concentration studies. A) View of set-up showing two fans facing the three cylindrical photoreactors. B) View of one cylindrical photoreactor comprised of a wash bottle that was cut open at both ends with a Waveform Lighting real UV LED strip wrapped along the interior of the cylinder.

Table S8. Measured Current of LED photoreactor for photon flux calculations.

Sample	Measured Current (amps)
Background	4.1×10^{-11}
LED 1	2.13×10^{-6}
LED 2	2.29×10^{-6}
LED 3	2.25×10^{-6}
LED 4	2.04×10^{-6}
LED 5	2.40×10^{-6}
Average	2.22×10^{-6}
Background subtracted average	2.22×10^{-6}
Multiplied by number of LEDs in photoreactor (120)	2.67×10^{-4}

The current for single LEDs from the LED strip were measured at the same distance from the photodiode as the sample distance in the photoreactor (3.5 cm). The average current measured for 5 LEDs was background subtracted from ambient light and multiplied by the number of LEDs in the photoreactor (120). Division of this current value by the responsivity of the photodiode used (0.05 amps/watt at 365 nm) gives the power of the LED strip in watts at the sample distance in the photoreactor (5.33×10^{-3}).

Solving for E in the equation for photon energy ($E = \frac{hc}{\lambda}$) with λ = 365 nm, gives a photon energy value of 5.45×10^{-19} J. Division of the measured wattage by the photon energy gives a photon flux value of 9.78×10^{15} photons/second delivered to the sample for all persistent radical studies.

Details of EPR experiment

For the measurement dried triply recrystallized samples were loaded in the quartz EPR tubes under argon (g) at room temperature and irradiated using 365 nm UV LEDs (9.78 X 10^{15} photons/s). Then the pre and post-UV irradiated EPR spectra at room temperature were compared. The EPR spectra were continuously monitored upon periodic 2 hours of UV irradiation while we observe no changes in the line shape or the width of the spectra further suggest the stability of the crystals. Then the radical concentration was approximated by comparing the area of the EPR spectra with a calibration curve of standard concentration of magic blue in dry methylene chloride (Figure S27). We continuously monitored the EPR spectra until observe a plateau in the radical concentration. From this comparison, the estimated radical concentration was 0.11% and 0.12% for two different trials of **1** using 8.1 mg and 7.7 mg of crystals. Next, the stability of the radical was estimated by dark decay study while keeping the sample in dark under argon (g) and monitored by EPR spectra over time.

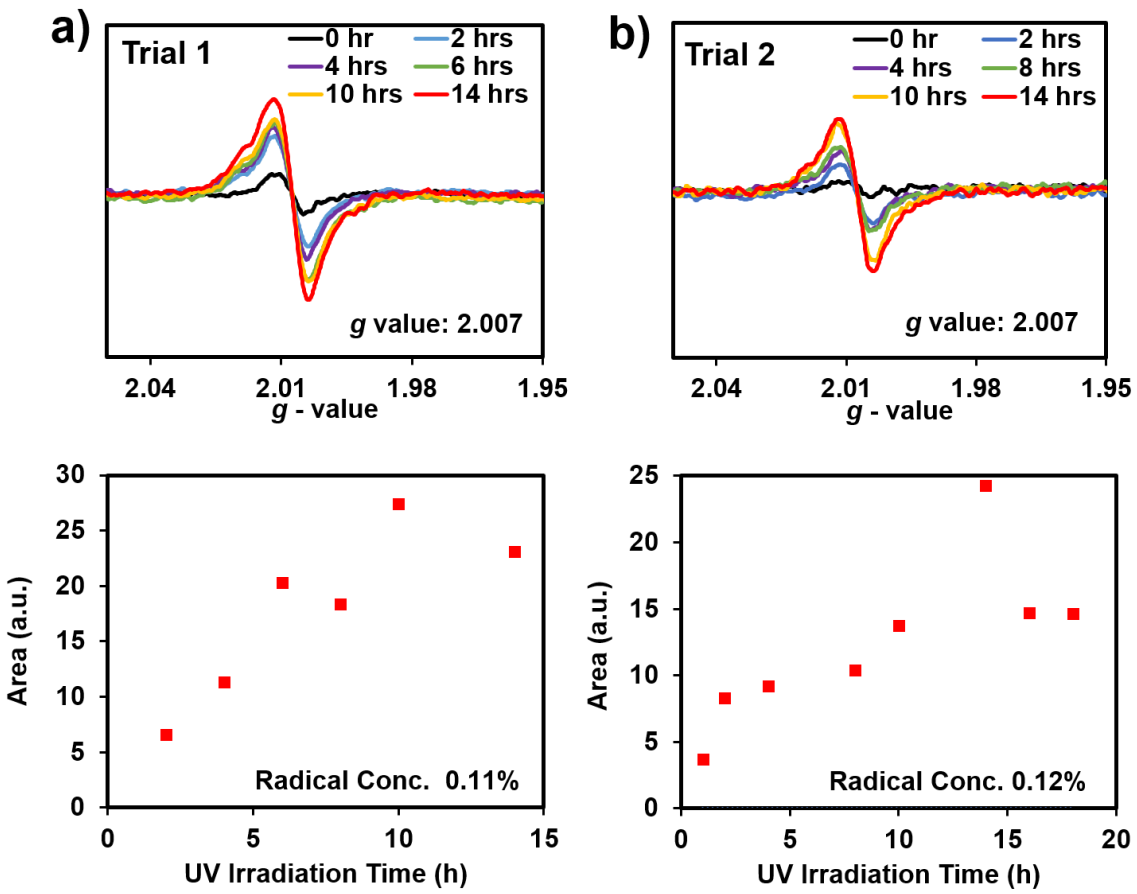

Figure S24. EPR data for the urea tethered TPA **1**. EPR spectra over time of UV irradiation (top). EPR spectra were doubly integrated to obtain the area plotted vs time of UV irradiation using 365 nm UV LED (bottom). a) Trial 1: A maximum radical concentration of 0.11% was obtained for 8.1 mg of triply recrystallized material by averaging last 3 data points. b) A maximum radical concentration of 0.12% was obtained for 7.7 mg of triply recrystallized material by averaging last 3 data points.

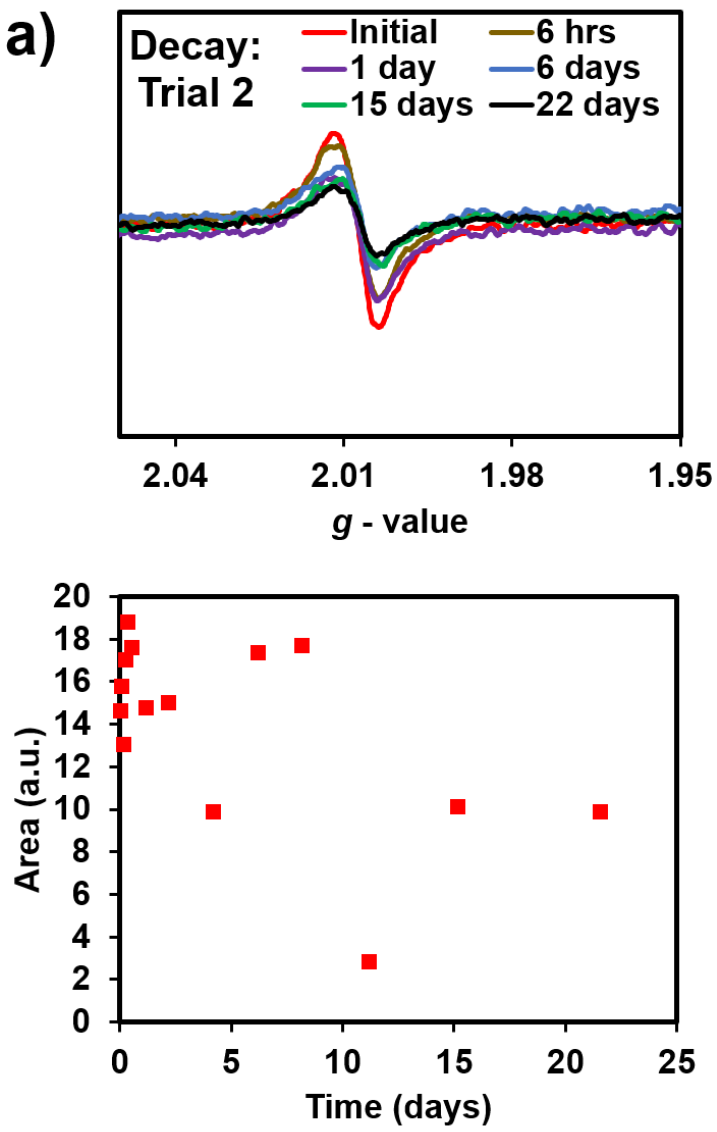

Figure S25. EPR data for **1**. EPR spectra over time (top) by keeping the UV irradiated sample under dark under the protection of argon. EPR spectra were doubly integrated to obtain the area plotted vs the time under dark (bottom)

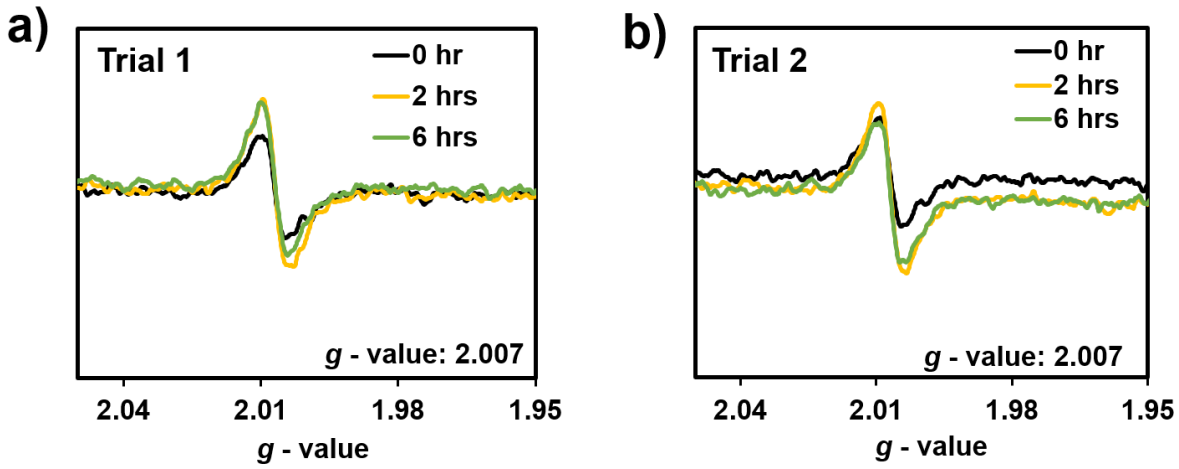

Figure S26. EPR data for the urea tethered **2**. EPR spectra over time of UV irradiation.) Trial 1: EPR spectra for triply recrystallized 6.4 mg of **2**. b) Trial 2: EPR spectra for triply recrystallized 6.1 mg of **2**. UV irradiation was performed using 365 nm UV LED source.

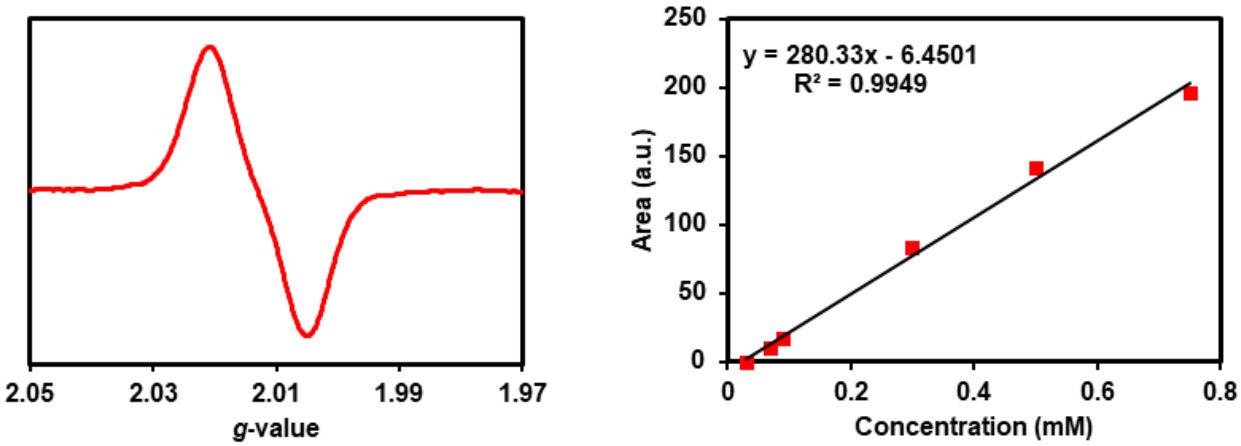

Figure S27. EPR data to determine the radical concentration using the calibration curve of magic blue. EPR spectra for 1 mM solution of magic blue in degassed dry dichloromethane (left) and calibration curve (right).

Computational Details for the simulation of absorption spectra in solution

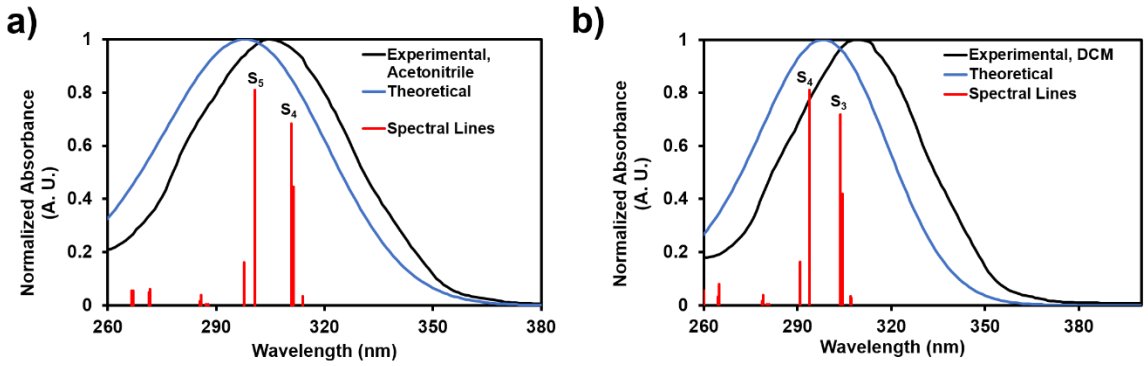

Figure S28. PCM solvation model to simulate the experimental absorption spectra of **1** in solution. a) Experimental absorption spectrum in acetonitrile. (inset black), theoretical absorption spectrum in acetonitrile (inset blue) and corresponding spectral lines (inset red). b) Experimental absorption spectrum in methylene chloride. (inset black), theoretical absorption spectrum in methylene chloride (inset blue) and corresponding spectral lines (inset red).

Polarizable Continuum Model (PCM): The implicit solvation model PCM was used to describe the effects of solvent dichloromethane (DCM), and acetonitrile on the absorption and structural properties of compound **1**. For this purpose, the ground-state geometry of **1** were optimized by using wB97XD[9]/LANL2DZdp methods in gas phase to avoid convergence error due to the presence of diffuse functions. The obtained geometry considered as energy minimum as corresponding frequencies were all positive. TD-DFT was applied to simulate the absorption spectra of methylene chloride and acetonitrile (using the ground state geometry) utilizing CAM-B3LYP/LANL2DZdp methods. 25 excited states were sufficient to reproduce the absorption spectra similar to the experimental absorption spectra. Only a shift of 7 nm and 11 nm was observed for acetonitrile and methylene chloride simulated absorption spectrum compared with experimental absorption spectrum. Therefore, CAM-B3LYP/LANL2DZdp method adequately describes the electronic structure of these urea tethered iodinated derivatives.

Table S9. Optimized geometry of **1** using ωB97X-D /6-31G* Methods in the gas phase

Atom	X (Å)	Y (Å)	Z (Å)
I	1.9251733	7.3622759	2.2067721
I	-5.3216789	-0.6963784	1.7364714
O	0.9032877	3.717482	11.940059
N	-1.145643	4.1173248	12.878764
H	-1.9558781	3.6279478	13.236487
N	-0.7987445	2.2104713	11.596228
H	-1.8072995	2.1900304	11.499612
N	-1.2583447	2.7525937	5.1243779
C	-0.2565949	3.3702223	12.123491
C	-0.0557742	1.4479379	10.603125
H	-0.2291883	0.3788578	10.778129
H	1.0046491	1.6490869	10.793307
C	-0.4026736	1.7926899	9.1679823
C	-0.4265451	3.1259484	8.7320857
H	-0.2032677	3.9265326	9.435932
C	-0.7274862	3.44214	7.4114194
H	-0.7502624	4.4824038	7.0936256
C	-0.9823849	2.4260069	6.4760138
C	-0.9525542	1.0920432	6.9015791
H	-1.1479044	0.293174	6.1896684
C	-0.6810914	0.7882948	8.2365624
H	-0.6684067	-0.2560285	8.5495061
C	-0.5365483	3.7882603	4.4831256
C	0.8343043	3.9657816	4.7177846
H	1.3566207	3.3024222	5.4034048
C	1.5357398	4.9891799	4.0805843
H	2.598827	5.1135395	4.2748337
C	0.8734134	5.8338862	3.185016
C	-0.4921948	5.6621613	2.9373464
H	-1.0178507	6.3184869	2.2475919
C	-1.1920022	4.651672	3.593303
H	-2.2566364	4.5250758	3.4090477
C	-2.1704983	1.9762218	4.3713557
C	-1.8663403	1.6074379	3.0530138
H	-0.9202113	1.9145028	2.6131848
C	-2.766007	0.856629	2.2990603
H	-2.5114333	0.581653	1.2785231
C	-3.9767043	0.4482806	2.8655167
C	-4.2883088	0.8002641	4.1832598
H	-5.2309437	0.4900246	4.6296084

C	-3.3920875	1.5673306	4.9265891
H	-3.6392725	1.8490784	5.9478171
I	-0.3396464	0.9476589	23.210891
I	8.8507848	3.6247678	18.0051
N	2.5406457	3.5924696	18.252403
C	-0.6226625	5.1915072	13.708555
H	-0.0172896	5.8449882	13.071999
H	-1.4831339	5.7784036	14.054943
C	0.2128945	4.7450382	14.896557
C	-0.1126511	3.6052152	15.638936
H	-0.9608742	2.9847942	15.350148
C	0.6535378	3.2150658	16.73545
H	0.3951387	2.3137574	17.28696
C	1.7576384	3.9806432	17.133713
C	2.0833415	5.1321355	16.404394
H	2.942597	5.7308129	16.699452
C	1.3257729	5.4944836	15.292435
H	1.6104738	6.3774116	14.720916
C	1.9112408	3.0118469	19.37854
C	0.7349267	3.571433	19.898753
H	0.3171149	4.4651945	19.440562
C	0.0931708	2.9881069	20.990008
H	-0.8208248	3.4333085	21.376584
C	0.6347316	1.8444808	21.585834
C	1.8162139	1.2877395	21.087689
H	2.243155	0.3955571	21.539732
C	2.4433969	1.8644935	19.9845
H	3.3531242	1.4183647	19.589136
C	3.9527843	3.6130208	18.174242
C	4.7089057	3.9598004	19.304094
H	4.2017726	4.2259475	20.228897
C	6.1005795	3.9583789	19.255224
H	6.6695327	4.2252637	20.142957
C	6.7542196	3.6296632	18.06283
C	6.0127714	3.3017823	16.924097
H	6.5110929	3.0408667	15.992755
C	4.6187815	3.2864735	16.984138
H	4.0453741	3.0168606	16.100057

Simulation of diffuse reflectance and details of electronic structure calculation

CAM-B3LYP is a hybrid exchange-correlation functional that combines the long-range correction (Coulomb Attenuation Method) with the popular hybrid functional B3LYP for better description of the charge-transfer excited states. The results obtained with CAM-B3LYP functional are reported in Tables S10-12 and in the main paper. The theoretical UV-vis spectra were generated as sums of Gaussian functions broadening of the spectral lines as given by equation 1.

$$g(x) = \sqrt{\frac{1}{\pi\sigma^2}} \sum_{\mathrm{n}} f_n \, \mathrm{e}^{-\frac{(x-x_n)^2}{\sigma^2}} \qquad (1)$$

In eqn (1), f_n and x_n stands for the oscillator strength and the position of the n^{th} line (in nm) respectively; x represents the energy variable in nm.

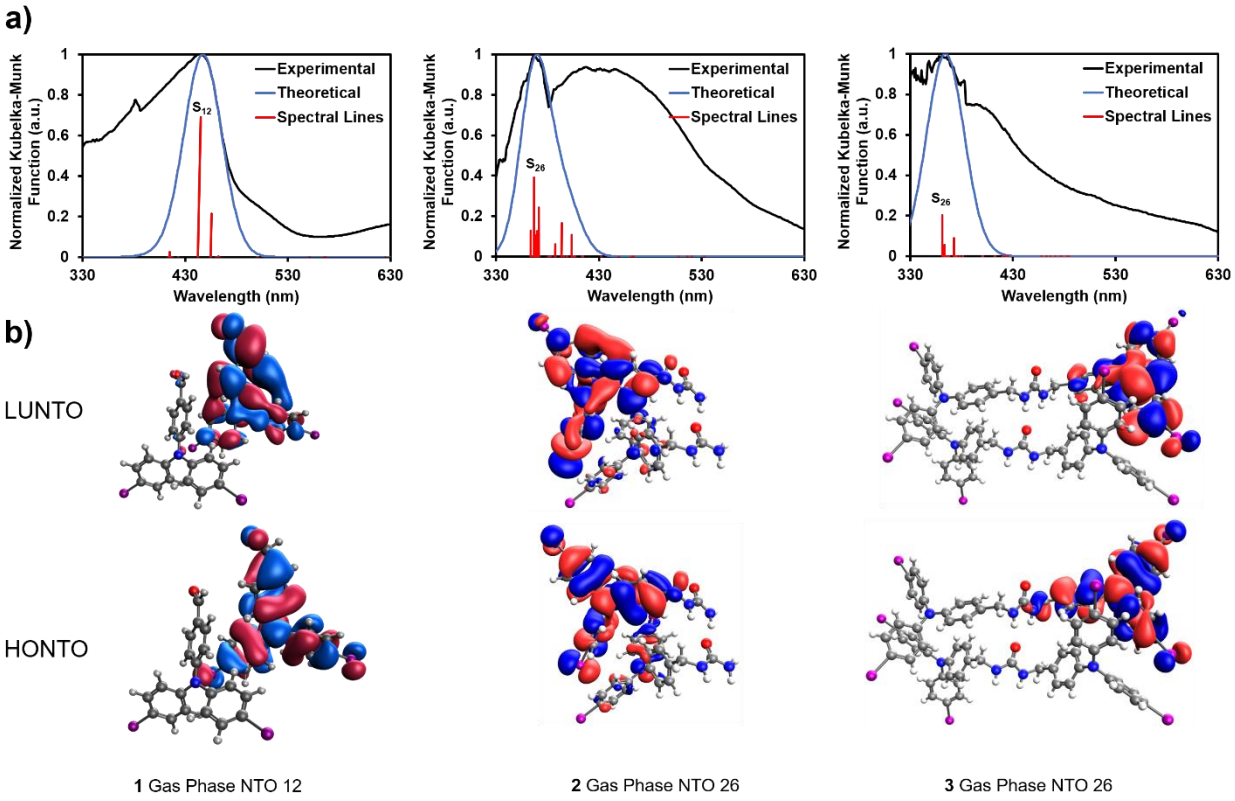

Figure S29. Comparison of normalized diffuse reflectance measurements, TD-DFT simulated spectra, and corresponding spectral lines. a) From left, transitions to the S_{12} state corresponds to the λ_{max} of **3** at 445 nm, transitions to the S_{26} state corresponds to the λ_{max} of **2** at 367 nm, transitions to the S_{26} state corresponds to the λ_{max} of **1** at 361 nm. b) Natural transition orbitals of **3**, **2**, and **1** in gas phase.

Table S10. Excited state transitions of hydrogen bonded dimer of **1** in the gas phase using CAM-B3LYP/LANL2DZdp methods implemented in TD-DFT. SC-XRD data of **1** were used as coordinates of heavy atoms. The energies were scaled by multiplying with 0.829 which were used to assign the spectral lines shown in Figure S29**.**

State	Energy (nm)	Oscillator Strength (f_{osc})
S_1	484	5.07E-07
S_2	482	1.5E-07
S_3	477	2.27E-06
S_4	476	4.93E-08
S_5	471	1.88E-07
S_6	466	1.16E-06
S_7	462	5.3E-07
S_8	457	5.65E-08
S_9	425	3.96E-08
S_{10}	423	5.28E-07
S_{11}	423	8.29E-07
S_{12}	422	2.37E-06
S_{13}	419	2.82E-07
S_{14}	412	2.24E-08
S_{15}	400	6.62E-08
S_{16}	399	7.89E-07
S_{17}	381	1.02E-07
S_{18}	377	9.14E-07
S_{19}	375	1.17E-07
S_{20}	374	8.38E-07
S_{21}	374	5.2E-06
S_{22}	373	4.02E-06
S_{23}	373	2.19E-06
S_{24}	372	0.088529
S_{25}	367	1.7E-06
S_{26}	365	8.01E-07
S_{27}	364	6.48E-05
S_{28}	363	5.03E-05
S_{29}	363	0.055991
S_{30}	361	0.203067

Table S11. Excited state transitions of hydrogen bonded dimer of **2** in the gas phase using CAM-B3LYP/LANL2DZdp methods implemented in TD-DFT. SC-XRD data of **2** were used as coordinates of heavy atoms. The energies were scaled by multiplying with 0.763 which were used to assign the spectral lines shown in Figure S29**.**

State	Energy (nm)	Oscillator Strength (f_{osc})
S_1	532	9.42E-08
S_2	520	4.91E-07
S_3	516	1.04E-07
S_4	507	5.86E-08
S_5	464	2.98E-07
S_6	462	5.54E-07
S_7	449	3.4E-09
S_8	432	6.78E-08
S_9	414	4.3E-09
S_{10}	413	2.24E-08
S_{11}	406	1.49E-07
S_{12}	405	2.28E-07
S_{13}	404	2.63E-07
S_{14}	403	0.10691
S_{15}	398	1.74E-08
S_{16}	396	2.45E-08
S_{17}	394	0.166528
S_{18}	387	0.061611
S_{19}	383	4.64E-07
S_{20}	380	3.84E-08
S_{21}	372	0.000143
S_{22}	371	8.25E-07
S_{23}	371	0.241359
S_{24}	370	0.000555
S_{25}	369	0.126994
S_{26}	368	0.105731
S_{27}	367	0.390429
S_{28}	366	1.01E-06
S_{29}	364	9.73E-06
S_{30}	363	0.127813

Table S12. Excited state transitions of dimer of **3** in the gas phase using CAM-B3LYP/LANL2DZdp methods implemented in TD-DFT. SC-XRD data of **3** were used as coordinates of heavy atoms. The energies were scaled by multiplying with 0.730 which were used to assign the spectral lines shown in Figure S29**.**

State	Energy (nm)	Oscillator Strength (f_{osc})
S_1	633	2.5E-07
S_2	625	3.32E-07
S_3	567	9.31E-07
S_4	565	3.3E-07
S_5	551	5.4E-09
S_6	551	2.82E-08
S_7	501	1.27E-06
S_8	499	7.2E-07
S_9	463	9.45E-08
S_{10}	462	0.001847
S_{11}	462	0.001399
S_{12}	459	1.86E-07
S_{13}	455	0.213675
S_{14}	445	0.690742
S_{15}	423	1.16E-07
S_{16}	423	6.8E-08
S_{17}	417	1.19E-07
S_{18}	415	2.79E-07
S_{19}	415	0.024467
S_{20}	413	9.72E-08

Electronic coupling calculation

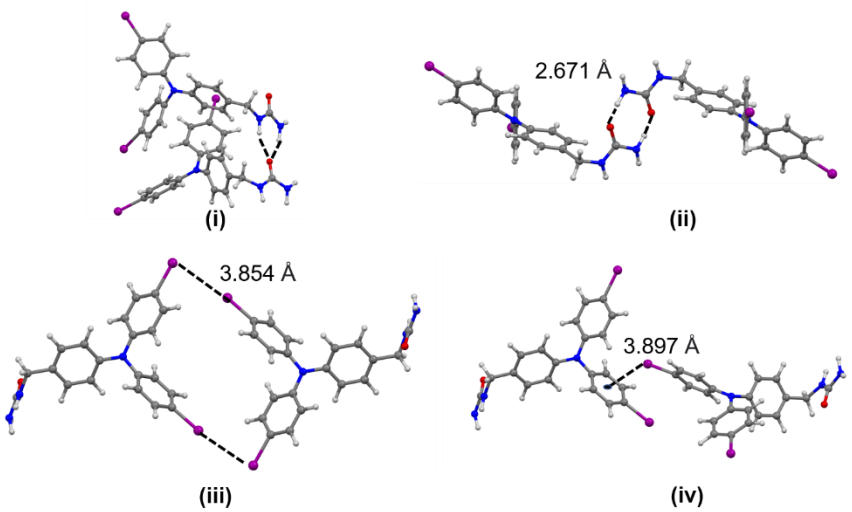

Figure S30. Dimer model of compound **2**

Table S13. The fragment charge difference for the dimer models of **2**

Dimer model	Method	dQ [a.u.]
i	CAM-B3LYP/LANL2DZdp	0.080099
ii	CAM-B3LYP/LANL2DZdp	-0.0022
iii	CAM-B3LYP/LANL2DZdp	0.000096
iv	CAM-B3LYP/LANL2DZdp	0.082568

Table S14. The LUMO gaps in eV for the dimer models of **2** computed within the Hartree-Fock theory for neutral geometry

Dimer model	Method	LUMO gap [eV]
i	def2-SVP	0.465
ii	def2-SVP	0.5
iii	def2-SVP	0.565
iv	def2-SVP	0.555

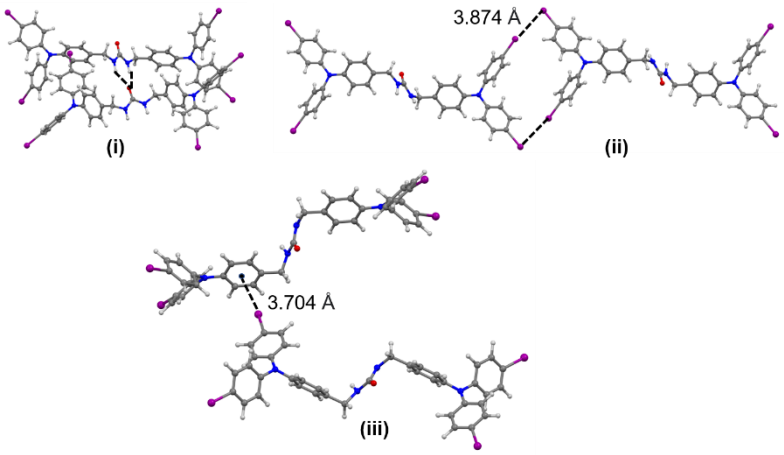

Figure S31. Dimer model of compound **1**

Table S15. The LUMO gaps in eV for the dimer models of **1** computed within the Hartree-Fock theory for neutral geometry

Dimer model	Method	LUMO gap [eV]
i	def2-SVP	0.125
ii	def2-SVP	0.119
iii	def2-SVP	0.125

Table S16. The LUMO gaps in eV for the dimer models of **2** computed within the Hartree-Fock theory for charged geometry

Dimer model	Method	LUMO gap [eV]
i	def2-SVP	0.16
ii	def2-SVP	0.087
iii	def2-SVP	0.089
iv	def2-SVP	0.089

Conductivity measurements for the Spiro-OMeTAD and 1 doped film samples

10 mg/ml of 1 was dissolved in a 1:1 mixture of Chlorobenzene and Chloroform (Sigma Aldrich, anhydrous) which also included 30 µL of a 170 mg/mL LiTFSI in Acetonitrile (Sigma Aldrich, anhydrous) solution and 10 µL of tert-butylpyridine (97% Sigma Aldrich). Spiro-OMeTAD solutions were prepared as is standard for perovskite solar cell deposition, i.e. 75 mg/mL in Chlorobenzene with the same additives as above. Both films were prepared via spin coating each mixture, where the solution was dropped on the spinning sample at 1500 rpm for 40s and a second step of 2000 rpm for 5s.

Table S17. Conductivity values obtained from the IV characteristic curves

Film sample	**Conductivity**
Spiro-OMeTAD	$(0.8 \pm 0.1) \times 10^{-6}$ S·cm^{-1}
1	$(2 \pm 1) \times 10^{-6}$ S·cm^{-1}

The vertical stack for conductivity measurements.

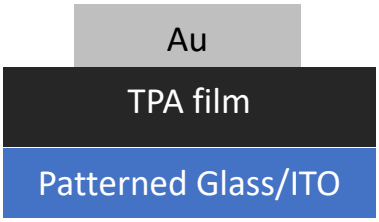

Experimental for film thickness measurement

For determining the thickness of film samples, the solution of the two materials were spin coated on glass substrates, and a thin scratch (~1mm wide) was etched/made after the samples dried. Thereafter, the sample thickness was measured by the surface profilometer.

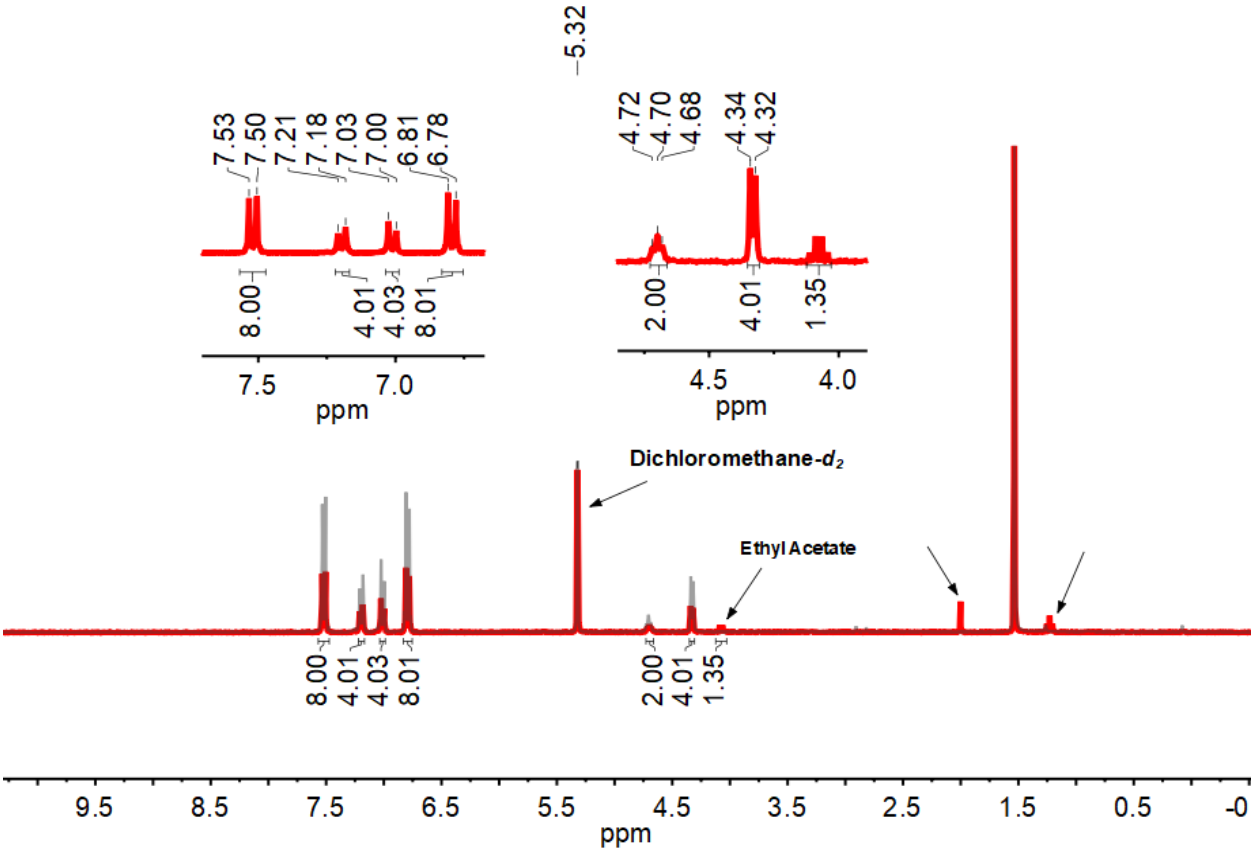

Figure S32. ^{1}H NMR spectra of compound **1** after EPR studies (CD_2Cl_2-d_2, 300 MHz) (red). ^{1}H NMR spectra of freshly synthesized compound **1** (black). EPR sample were dissolved in NMR solvent prior measurement. Integrals and peaks are the for the **1** after EPR experiments. No changes were observed after EPR experiments. We observe the presence of encapsulate ethyl acetate with a host-guest ratio 3: ethyl acetate = 1 : 0.68 compared to the ratio of SC-XRD 1 : 0.72.

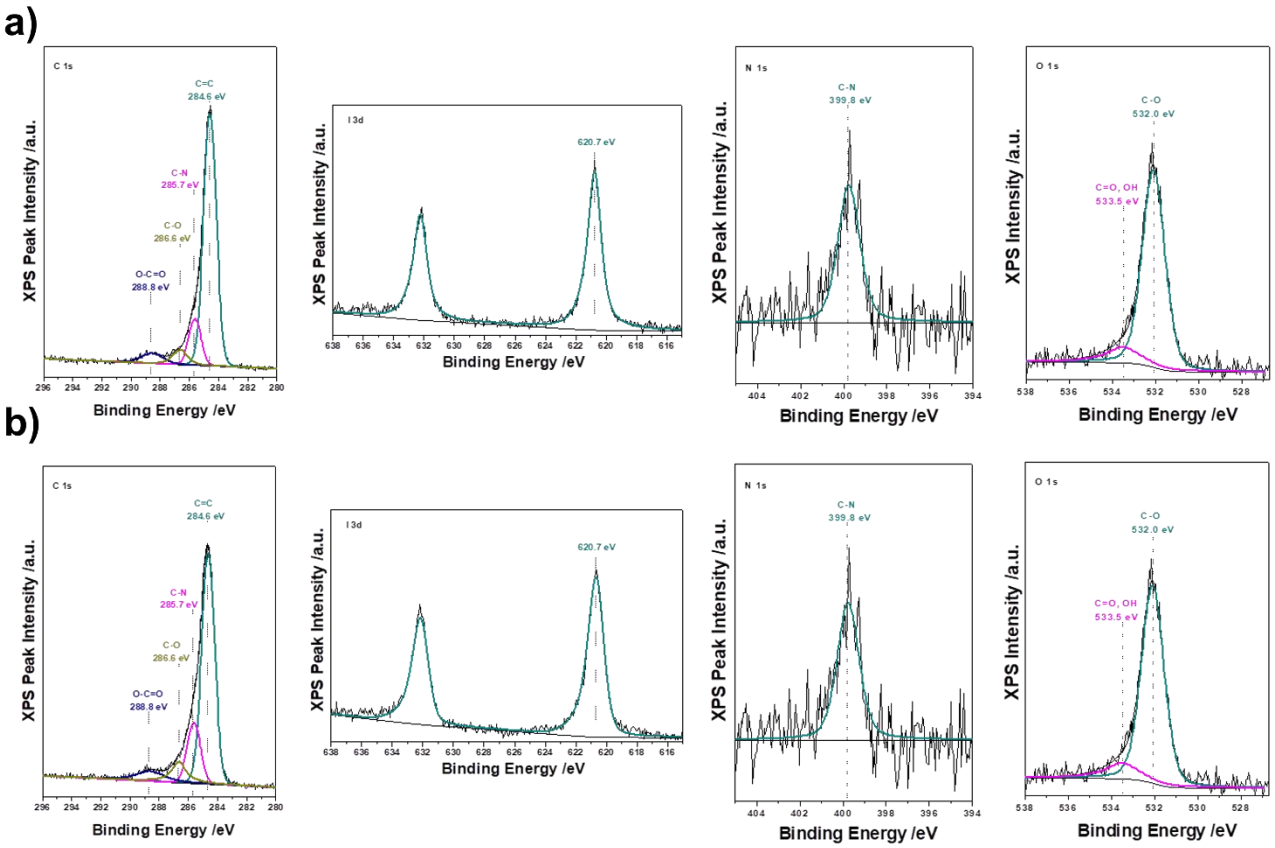

Figure S33. XPS analysis on pre and post-UV irradiated crystalline sample of **1**. UV irradiation was performed in situ (24 hours) a) Binding energy of XPS core level peaks (from left) C 1s, I 3d, N 1s, O 1s pre-UV irradiation. b) Binding energy of XPS core level peaks (from left) C 1s, I 3d, N 1s, O 1s post UV irradiation. No changes or shift were observed in the binding energy of the core level peaks compared with the post-UV irradiated sample. These XPS results can be attributed to the stability of the crystalline **1** during UV irradiation.

References

1 X. Wu, M. Jin, J. Xie, J.-P. Malval and D. Wan, *Chem. - A Eur. J.*, 2017, **23**, 15783–15789.

2 A. J. Sindt, B. A. DeHaven, D. W. Goodlett, J. O. Hartel, P. J. Ayare, Y. Du, M. D. Smith, A. K. Mehta, A. M. Brugh, M. D. E. Forbes, C. R. Bowers, A. K. Vannucci and L. S. Shimizu, *J. Am. Chem. Soc.*, 2020, **142**, 502–511.

3 H. Tian, X. Yang, R. Chen, R. Zhang, A. Hagfeldt and L. Sun, *J. Phys. Chem. C*, 2008, **112**, 11023–11033.

4 G. G. Dubinina, R. S. Price, K. A. Abboud, G. Wicks, P. Wnuk, Y. Stepanenko, M. Drobizhev, A. Rebane and K. S. Schanze, *J. Am. Chem. Soc.*, 2012, **134**, 19346–19349.

5 APEX3 Version 2016.5-0 and SAINT+ Version 8.37A. Bruker AXS, Inc., Madison, Wisconsin, USA, 2016.

6 SADABS-2016/2: L. Krause, R. Herbst-Irmer, G. M. Sheldrick and D. Stalke, *J. Appl. Cryst*, 2015, **48**, 3–10.

7 (a) SHELXT: G. M. Sheldrick, *Acta Crystallogr. Sect. A*, 2015, **A**, 3–8. (b) SHELXL: G. M. Sheldrick, *Acta Crystallogr. Sect. C Struct. Chem.*, 2015, **71**, 3–8.

8 OLEX2: O. V. Dolomanov, L. J. Bourhis, R. J. Gildea, J. A. K. Howard and H. Puschmann, *J. Appl. Crystallogr.*, 2009, **42**, 339–341.

9 J. Da Chai and M. Head-Gordon, *Phys. Chem. Chem. Phys.*, 2008, **10**, 6615–6620.